Paulo Roberto Matias Júnior

Optimum Design of Modular Multilevel Converters for Variable-Speed Electrical Drives

Belo Horizonte, MG

2021

Paulo Roberto Matias Júnior

Optimum Design of Modular Multilevel Converters for Variable-Speed Electrical Drives

Dissertação submetida à banca examinadora designada pelo Colegiado do Programa de Pós-Graduação em Engenharia Elétrica do Centro Federal de Educação Tecnológica de Minas Gerais e da Universidade Federal de São João Del Rei, como parte dos requisitos necessários à obtenção do grau de Mestre em Engenharia Elétrica.

Centro Federal de Educação Tecnológica de Minas Gerais

Programa de Pós-Graduação em Engenharia Elétrica

Orientador: Prof. Dr. Allan Fagner Cupertino

Coorientador: Prof. Dr. Heverton Augusto Pereira

Belo Horizonte, MG

2021

Matias Júnior, Paulo Roberto

M433o Optimum design of modular multilevel converters for variable-speed electrical drives / Paulo Roberto Matias Júnior. – 2021.

93 f.: il., gráfs, tabs.

Dissertação de mestrado apresentada ao Programa de Pós-Graduação em Engenharia Elétrica em associação ampla entre a UFSJ e o CEFET-MG.

Orientador: Allan Fagner Cupertino.

Coorientador: Heverton Augusto Pereira.

Dissertação (mestrado) – Centro Federal de Educação Tecnológica de Minas Gerais.

1. Máquinas elétricas – Controle – Teses. 2. Conversores – Teses. 3. Energia elétrica – Conservação – Padrões – Teses. 4. Energia elétrica – Transmissão – Confiabilidade – Teses. I. Cupertino, Allan Fagner. II. Pereira, Heverton Augusto. III. Centro Federal de Educação Tecnológica de Minas Gerais. IV. Universidade Federal de São João del-Rei. V. Título.

CDD 621.313

Elaboração da ficha catalográfica pela bibliotecária Jane Marangon Duarte, CRB 6º 1592 / Cefet/MG

À minha família, amigos e mestres.

Agradecimentos

Em primeiro lugar agradeço a Deus por ter possibilitado que eu chegasse até aqui e ter me dado forças para batalhar por esse sonho. Agradeço e dedico essa vitória a minha mãe, Josiene, o meu porto seguro, pelo amor incondicional, por abdicar de seus planos para que pudesse ir atrás do meu sonho e para isso não mediu esforços. Ao meu querido pai, Paulo, que mesmo não estando presente fisicamente me guardou e me fortaleceu e onde estiver sei que está imensamente contente e orgulhoso por essa conquista. A minha irmã, Thamires, pelos conselhos e por sempre estar de prontidão quando preciso. A minha namorada, Júlia, por sempre estar ao meu lado, pelas palavras de incentivo e cumplicidade. Agradeço aos amigos e familiares que andaram ao meu lado e me alegraram em momentos difíceis, me deram força e companhia para vencer cada desafio. Ao meu querido afilhado, Anthony, pela imensa alegria diária. Agradeço também aos meus orientadores, Allan, pelos diversos ensinamentos (muitas vezes com reuniões adentrando a madrugada quando estava Dinamarca), pelo incentivo, pela confiança, compreensão e pela motivação quando os resultados pareciam distantes. Certamente sem o seu auxílio o caminho seria MUITO mais árduo e sinuoso. Ao Heverton, pelo apoio e conselho nos momentos certos, pela oportunidade de me qualificar e estar podendo buscar o título de mestre e todos os ensinamentos durante a trajetória da graduação e do mestrado. Aos queridos amigos do GESEP, mesmo estando mais distante nesses últimos anos, sempre estão de prontidão com todo companheirismo e apoio. Obrigado a todos que cruzaram meu caminho e me ajudaram a trilha-lo. Cada obstáculo nesses cinco anos de graduação me formaram o que sou hoje, o meu crescimento veio por cada um deles. Muito obrigado!

"Experience is not what happens to you,
it's what you do with what happens to you."
(Aldous Huxley)

Resumo

O conversor modular multinível (CMM) é uma topologia inerentemente tolerante a falhas e uma opção interessante para acionamentos elétricos de média tensão, especialmente quando cargas quadráticas são empregadas. Para selecionar a melhor tensão de bloqueio de IGBTs, este trabalho apresenta uma metodologia de projeto e comparação de CMMs considerando a redundância necessária para atingir o requisito de confiabilidade. São comparados projetos utilizando IGBTs comerciais com tensão de bloqueio na faixa de 1,7 a 6,5 kV. A seleção é baseada em métricas de complexidade, volume, área de silício e eficiência do conversor. O uso da metodologia é exemplificado por meio de um estudo de caso de um soprador industrial acionado por um motor de indução trifásico de 13,8 kV - 16 MW. Medições da velocidade de operação do acionamento e temperatura ambiente desse processo em uma indústria siderúrgica localizada no sudeste brasileiro são utilizadas na avaliação das perdas do conversor. Os resultados evidenciam que a classe de tensão ótima de IGBTs depende do tipo de redundância empregado. Além disso, apesar do aumento de complexidade e do número de componentes, os projetos baseados em IGBTs com menor tensão de bloqueio (1,7 e 3,3 kV) se mostram mais vantajosos devido a menores perdas, volume ocupado pelo conversor e área de silício.

Palavras-chaves: Acionamentos Elétricos; Conversor Modular Multinível; Projeto Otimizado; Confiabilidade.

Abstract

The modular multilevel converter (MMC) is an inherently fault-tolerant topology and an interesting option for medium voltage electrical drives, especially when quadratic loads are taken into account. In order to select the optimal blocking voltage for IGBTs, this work presents a design methodology and comparison of MMCs considering the necessary redundancy to achieve the reliability requirement. Designs using commercial IGBTs with blocking voltage in the range of 1.7 to 6.5 kV are compared. The selection is based on complexity, volume, silicon area and efficiency. The methodology application is exemplified through an industrial blower driven by a 13.8 kV - 16 MW three-phase induction motor. Measurements of the operating drive speed and ambient temperature of this process, which is part of a steel industry located in southeastern Brazil, is used as mission profile. The results show that the optimal class of IGBTs depends on the type of redundancy employed. In addition, despite the increase in complexity and the number of components, designs based on IGBTs with lower blocking voltage (1.7 and 3.3 kV) are proved to be more advantageous due to lower losses, converter volume and silicon area.

Key-words: Electric Drive; Modular multilevel converter; Optimal Design; Reliability.

List of Figures

List of Tables

List of abbreviations and acronyms

ABB	Asea Brown Boveri (Swedish-Swiss multinational corporation)
ac	Alternating Current
ALO	Arithmetic and Logical Operations
ANPC	Active Neutral Point Clamped
BESS	Battery Energy Storage Systems
CCV	Cycloconverter
CHB	Cascaded H-bridge Converter
CM	Common-Mode
CMI	Common-Mode Injection
COBEP	Brazilian Power Electronics Conference (Conferência Brasileira de Eletrônica de Potência)
CSC	Current Source Converter
CSPI	Cooling System Performance Index
dc	Direct Current
EMI	Electromagnetic Interference
FB	Full-Bridge
FCMC	Flying Capacitor Multilevel Converter
FIT	Failure in Time
GCT	Gate Comutated Thyristor
GESEP	Power Electronics and Power Systems UFV laboratory (Gerência de Especialistas em Sistemas Elétricos de Potência)
GTO	Gate Turn-Off Thyristor
HB	Half-Bridge
HVDC	High-Voltage Direct Current

IEEE	Institute of Electrical and Electronics Engineers
IGBT	Insulated Gate Bipolar Transistor
IGCT	Insulated Gate Comutated Thyristor
LCI	Load-Comutated Inverter
MAF	Moving Average Filter
MATLAB	Matrix Laboratory
MC	Matrix Converter
MMC	Modular Multilevel Converter
NPC	Neutral Point Clamped
PCC	Point of Common Coupling
PI	Proportional Controller
PI	Proportional Integral Controller
PLECS	Piecewise Linear Electrical Circuit Simulation
PR	Proportional Resonant Controller
PS-PWM	Phase-Shifted Pulse Width Modulation
pu	Per Unit
PWM	Pulse Width Modulation
PWM-CSI	Pulse Width Modulated Current Source Inverter
rms	Root Mean Square
SCR	Silicon Controlled Rectifier
SDW	WEG Design Software (Software de Dimensionamento WEG)
SM	Submodule
RFOC	Rotor Field Oriented Control
RAS	Redundant Operation Based on Additional SMs
RASO	Optimized Redundant Operation Based on Additional SMs
RS	Standart Redundant Operation

RSS	Redundant Operation Based on Spare SMs
STATCOM	Static synchronous compensator
VSC	Voltage Source Converter
VSDs	Variable Speed Electric Drives
WEG	WEG S.A (Brazilian multinational corporation)

List of symbols

C	SM capacitance
C_v	Volume compensation factor
D_1	Bottom diode
D_2	Top diode
E_C	Stored energy
F	Number of failure SMs per arm
f^*_{com}	Common-mode frequency
f_{ef}	Effective output frequency
f_r	Redundancy factor
f_s	Frequency of the voltage applied in the motor
$f_{s,r}$	Stator rated frequency
f_{sw}	Carrier frequency
f_u	Utilization factor
f_{us}	Semiconductor utilization factor
$f_{us,0}$	Semiconductor utilization factor under normal conditions
$f_{us,f}$	Semiconductor utilization factor under failure conditions
i_{arm}	Arm current
I_c	Rated collector current of the device
i_{ds}	Stator direct current
i^*_{ds}	Stator direct current reference
i_l	Lower arm current
i_{qs}	Quadrature direct current
i^*_{qs}	Quadrature direct current reference

i_s	Stator current
I_s	Stator rms current
$I_{s,r}$	Stator rms rated current
$i^*_{sm,i}$	SM current
i_u	Upper arm current
i^*_{zac}	Common-mode circulating current
i^*_z	Circulating current reference
K	Coupling coefficient
$k_{compl.}$	Complexity normalized index
K_E	Volume per stored energy constant
$k_{effic.}$	Efficiency normalized index
k_{res}	Percentage of reserve voltage
$k_{sil.a.}$	Silicon area normalized index
k_u	Perceptual variation in the utilization factor
$k_{vol.}$	Volume normalized index
k_t	Normalized total index
k_x	Normalized index
L_1	Winding 1 inductance
L_2	Winding 1 inductance
L_{arm}	Arm inductance
$L_{arm,s}$	Equivalent inductance seen from the motor current side
$L_{arm,z}$	Equivalent inductance seen from the circulating current side
L_m	Magnetization inductance
L_lr	Rotor leakage inductance
L_ls	Stator leakage inductance
L_s'	Stator transient inductance

M	Number of redundant SMs per arm
$M_{1,2}$	Mutual inductance of L_1 that exerts in L_2
$M_{2,1}$	Mutual inductance of L_2 that exerts in L_1
N	Number of effective SMs per arm
M_w	Mutual inductance between L_1 and L_2
N_1	Number of turns of the winding 1
N_2	Number of turns of the winding 2
$n_{m,r}$	Motor rated speed
$N_{o,l}$	Number of operating SMs of the lower arm
$N_{o,u}$	Number of operating SMs of the upper arm
N_{semi}	Number of semiconductors
N_T	Total number of operating SMs per phase
N_w	Number of turns of the winding
P	Number of poles
P_r	Rated active power of the motor
P_{sw}	Switched power
$\Re_c$	Reluctance of core
$\Re_1$	Reluctance of core 1
$\Re_1$	Reluctance of core 2
$R_{active}(t)$	Arm level reliability function considering the active mode redundancy
R_{arm}	Arm inductor resistor
R_b	Bleeder resistor
R_{heat}	Heatsink thermal resistance
$R_{MMC,active}(t)$	System level reliability function considering the active mode redundancy
$R_{MMC,standby}(t)$	System level reliability function considering the standby mode redundancy

R_r	Rotor resistance
R_s	Stator resistance
$R_{standby}(t)$	Arm level reliability function considering the standby mode redundancy
$R_{sm}(t)$	SM Reliability function
$R(t)$	Reliability function
S_1	Bottom IGBT
S_2	Top IGBT
S_n	MMC apparent power
S_T	Bypass switch
T_a	Ambient temperature
T_c	Case temperature
T_e	Electrical torque
T_h	Heatsink temperature
T_j	Junction temperature
T_L	Load torque
T_{max}/T_{rated}	Ratio between maximal and rated torque
V_{AB}	AB voltage
$V_{AB,s}$	AB voltage seen from the motor current side
$V_{AB,z}$	AB voltage seen from the circulating current side
v_{avg}	SM average voltages
v_{avg}^*	SM average voltages reference
v_b^*	Balancing voltage reference
V_{bv}	Blocking voltage
$V_{bv,100fit}$	Blocking voltage for a device failure rate of 100 failures in time
V_{cap}	Capacitor volume
v_{com}^*	Common-mode voltage

V_{com}^*	Common-mode rms voltage
v_{dc}	dc-link voltage
V_{heat}	Heatsink volume
V_{IGBT}	IGBT volume
v_l^*	Lower arm reference voltage
V_s	Stator rms voltage
$V_{s,r}$	Stator rated voltage
v_s^*	Stator reference voltage
v_{sm}^*	SM reference voltage
$v_{sm,f}$	Filtered SM voltage
$v_{sm,i}$	SM voltage
v_u^*	Upper arm reference voltage
v_z^*	Internal voltage reference
W_{conv}	Energy storage requirement
x	Metric used
x_{max}	Maximum value of the metric used
x_{min}	Minimum value of the metric used
Z_{c-h}	Case-to-heatsink thermal impedance
Z_{h-a}	Heatsink-to-ambient cooling thermal impedance
$Z_{j-c,cauer}$	Junction-to-case Cauer thermal impedance
$Z_{j-c,foster}$	Junction-to-case Foster thermal impedance
β	Angular displacement between the carrier waveforms in the upper and lower arms
Δi_z	Circulating current ripple
Δv_{sm}	Capacitor voltage ripple
$\Delta \omega_m$	Speed error

$\lambda(t)$	Failure rate
$\lambda_{capacitor}$	Capacitor Failure rate
$\lambda_{control}$	Control system Failure rate
λ_{IGBT}	IGBT Failure rate
λ_{sm}	SM Failure rate
$\theta^i_{c,l}$	Angular displacements of the lower carrier waveforms
$\theta^i_{c,u}$	Angular displacements of the upper carrier waveforms
θe	Electrical angle
ω^*_{com}	Common-mode angular frequency
ω_e	Electrical frequency
ω_m	Motor speed
ω^*_m	Motor reference speed

Superscripts

$*$	Reference value

Subscripts

u	Upper arm
l	Lower arm
a	a-phase
b	b-phase
c	c-phase

Contents

1 Introduction

1.1 Context and Relevance

The continuous increase in demand and the cost of electric energy proves that the energy must be used more efficiently and rationally. In this way, efficiency has become a major figure of merit in today's industry, due to its economic benefits and also the importance of sustainability (Abu-Rub et al., 2016). Most of the electricity used in the industry sector is for electrical drive systems. Motor systems currently account for 30% of global electricity demand (IEA, 2019).

Driven by the economy of scale and higher production rates, variable speed electric drives (VSDs) are increasingly present in the industrial field, bringing several advantages such as energy savings, soft starts, greater reliability and safety (Rodriguez; Jih-Sheng Lai; Fang Zheng Peng, 2002; Tai et al., 2017). Other factors that contributed to this recent trend change are technological developments in power electronics field, the increase in the reliability of converters and the fact that life cycle costs (initial cost + operating cost) become more important than the initial investment, especially when it comes to medium-voltage and high-power applications (Kouro et al., 2012).

Medium-voltage drives have found extensive applications in several sectors, such as in the oil and gas, petrochemical, mining, water/waste, cellulose/paper, cement, chemical, power generation, metal production and processes, traction and marine drives sectors (Okayama et al., 1996; Bernet, 2000; Steinke; Steimer, 2000; Schmitt; Sommer, 2001; Issouribehere et al., 2008; Andonov et al., 2012; Liang; Kar; Liu, 2015). Table 1 shows various medium-voltage drive applications along with the respective power ranges and

Table 1 – Industry applications of medium-voltage drives (Klug; Klaassen, 2005; Kouro et al., 2012).

Industry Sector	**Application**	**Power Range**
Chemical, Cement	Extruders, pumps, compressors, blowers, cement mills, fans, mixers, presses	0.5 - 4 MW
Mining	Ore mills, mine hoists, conveyor belts, pumps, crushers, blowers, compressors, excavators	2 - 15 MW
Marine	Propulsion drives, booster-generators, thrusters, winders, dredge pumps	2 - 20 MW
Metal	Rolling mills, sectional steel mill, blast furnace converter	2 - 25 MW
Water	Pumps, blowers	0.5 - 40 MW
Oil and gas	Compressors, centrifugal pumps	1 - 80 MW

industry sector. Medium-voltage inverters cover power ratings from 0.5 to 80 MW at the medium-voltage level of 2.3–13.8 kV (Abu-Rub; Iqbal; Guzinski, 2012). However, the majority of installed medium-voltage inverters are in the 1–4 MW range with voltage ratings of 3.3 to 6.6 kV, according Fig. 1 (a). Market share research has shown that about 70% of medium-voltage inverter applications are for pumps and fans, as shown in Fig. 1 (b) (Wu; Narimani, 2017).

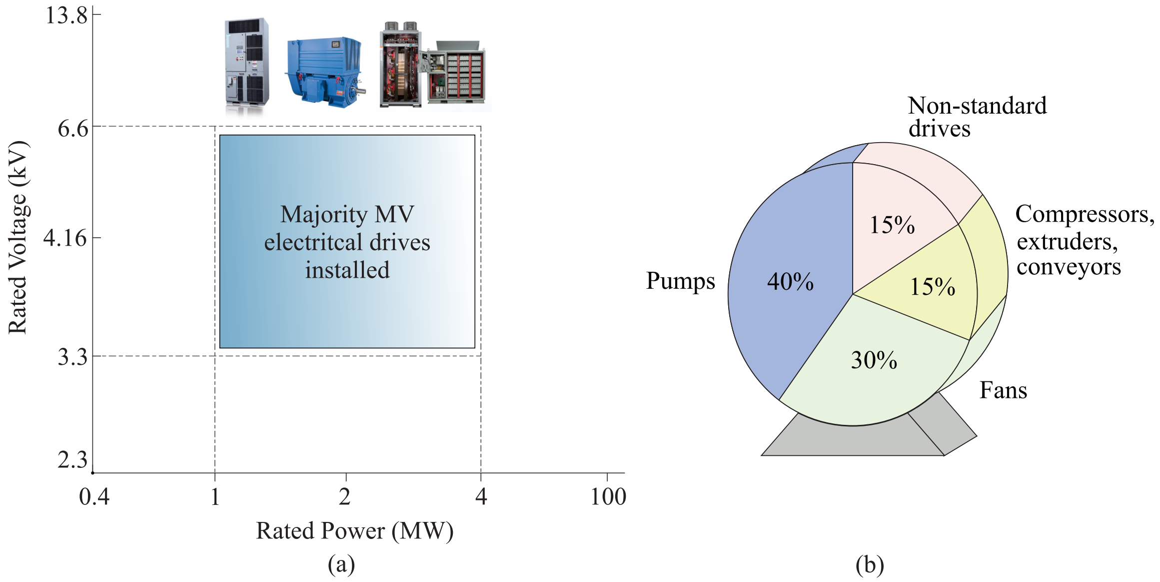

Figure 1 – Market share of the medium-voltage electrical drives: (a) Voltage and power ranges; (b) Typical applications. *Adapted from*: (Wu; Narimani, 2017)

One of the main markets for the medium-voltage inverter is for retrofit applications. Although with advances in high-power converter technology and variable-speed medium-voltage drives have been widely accepted in the industry in the past three decades, many of the medium-voltage motors still operate at a fixed speed (Wu; Narimani, 2017). When large fans, pumps or compressors are driven by a fixed speed motor, the control of air or liquid flow is usually achieved by mechanical methods, resulting in a large amount of energy loss. The use of adjustable speed medium-voltage inverters ensures significant energy savings, up to 30%, and reduces the return on investment by up to 2.5 years (Abu-Rub et al., 2016). Furthermore, transformerless solutions lead to an even greater reduction in payback time (Abu-Rub; Malinowski; Al-Haddad, 2014).

However, the implementation of such medium-voltage electrical drives is associated with several requirements and challenges. These challenges can be divided into 4 groups which are summarized in Fig. 2: the power quality requirements on the point of common coupling (PCC), the challenges associated with the design of the converter on the motor-side, the restrictions of the semiconductor devices, and finally the requirements of the electric drive system (Wu; Narimani, 2017).

Regarding to the PCC, there is a concern with power quality. The distortion of

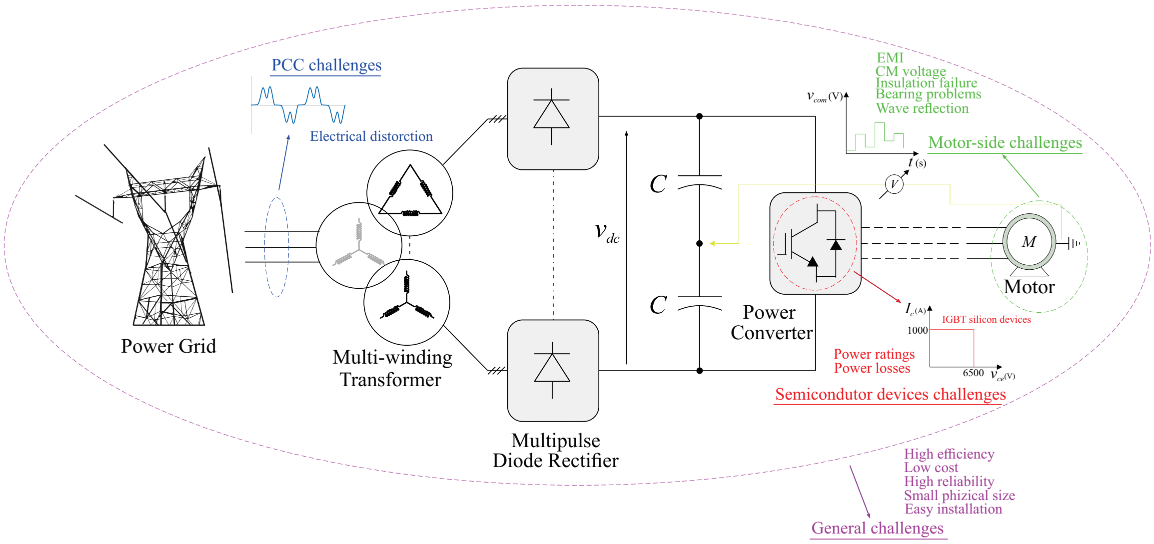

Figure 2 – Challenges of the medium-voltage electrical drives.

electrical variables due to the input rectifier can cause several problems, such as overheating of transformers, equipment failure and malfunction of communications equipment (Abu-Rub et al., 2016). In addiction, the harmonics on the converter output require financial investment to fix, and may generate penalties from the utility. One possible way to overcome this problem can be overcome by using multi-pulse rectifiers, improving the power quality at the PCC.

In motor-side, problems caused by converter can be catastrophic. The switching of semiconductor devices results in high dv/dt and a common-mode voltage (Zhu et al., 2013). Depending on the dc-link voltage, the dv/dt and the common-mode voltage can cause premature failure of the motor insulation and winding, bearing problems, electromagnetic interference (EMI) and wave reflection. As a consequence, the life expectancy of the electrical motor is reduced (Tolbert; Fang Zheng Peng; Habetler, 1999).

In semiconductor devices, the conduction and switching losses are responsible for a significant amount of the total energy loss in the medium-voltage converter (Ben-Brahim et al., 2019). Minimizing losses can lead to a reduction in the operating cost of the inverter. Reducing the switching frequency, generally causes an increase in the harmonic distortion of the waveforms on the PCC and motor-side, but reduces switching losses. In this way, a good design must be made to choose the best switching frequency to have lower losses and minimize harmonic distortions (Abu-Rub et al., 2016). Another challenge linked to semiconductor devices is the voltage rating. For silicon IGBTs, the blocking voltage is limited to 6.5 kV. One way to get around this is to use series devices. Since devices connected in series and their gate drivers may not have identical characteristics, they may not equally share the voltage in blocking state or during switching transients (Stemmler; Guggenbach, 1993; Abu-Rub et al., 2010). This fact justifies the use of multilevel topologies.

Finally, the general requirements for the medium-voltage drive system include high efficiency, low manufacturing cost, small physical size, high reliability, effective failure protection, easy installation and minimum downtime for repairs. Some of the application-specific requirements include high dynamic performance, regenerative braking capacity and four-quadrant operation (Klug; Klaassen, 2005; Abu-Rub et al., 2016; Wu; Narimani, 2017).

1.2 Purpose and Contributions

Medium-voltage electric drives play an important role in the industry and have high availability, leading to energy saving and soft start (Rodriguez; Jih-Sheng Lai; Fang Zheng Peng, 2002; Tai et al., 2017). Among the emerging topologies for medium voltage drives, the Modular Multilevel Converter (MMC) has become a interesting solution for medium-voltage and high power drives based pumps, fans and compressors applications (Kouro et al., 2012; Abu-Rub et al., 2016). As shown in Fig. 1 (b) these applications account for up to 70% of the medium-voltage electrical drives. Its main features of the MMC include low dv/dt, high efficiency, modularity, low harmonic distortion in the output variables and inherent redundancy (Kouro et al., 2010; Hagiwara; Hasegawa; Akagi, 2013; Antonopoulos et al., 2014; Pan et al., 2020). Companies like Siemens and Benshaw commercialize the MMC topology for pumps, fans and compressors applications (Akagi, 2017). This topology has proven to be a interesting candidate for high-voltage direct current systems (HVDC) and static synchronous compensators (STATCOM) (Dekka et al., 2017).

The benefits of the MMC-based electric drives have increased the interest for researchers. In terms of publications, Fig. 3 presents the number of published journal papers on this topic since 2011. These data are obtained searching the term “Modular Multilevel Converter Based Drives” in IEEE Xplore and Science Direct databases. As observed, modular multilevel converters have been widely investigated in last 4 years.

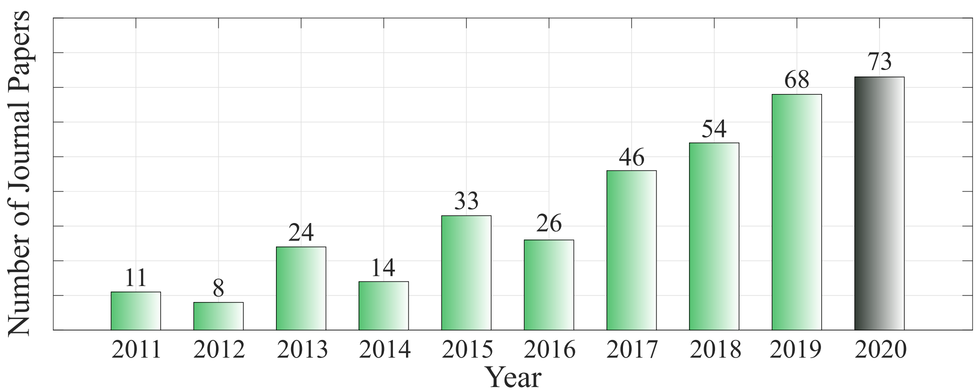

Figure 3 – Evolution of the number of published journal papers containing the term ”Modular multilevel converters based drives” in IEEE Xplore and Science Direct databases.

An important issue in the MMC design is the blocking voltage of commercially available power IGBTs in the market, ranging from 0.6 to 6.5 kV (Huber; Kolar, 2017). Some papers evaluate the optimal converter design for a given application, voltage and power rating. Reference (Islam; Guo; Zhu, 2014a) proposes the design of a cascade converter for renewable energy integration, taking into account system performance, control complexity and semiconductor cost. The results show that the 19 level topology is the optimal choice for an 11-kV power conversion system. In (Siddique et al., 2016), the MMC and 3L-NPC converter are compared for battery energy storage system (BESS). The comparison is based on number of power modules, ratings, the filter elements, system efficiency, harmonic content and investment cost. Marzoughi et al. (2018) presents the design procedure and comparison of power converters used in medium-voltage drives for different voltage and power levels, however, the ripple mitigation strategy at low speeds is not considered. Finally, Islam, Guo and Zhu (2014a) proposes to determine the optimal blocking voltage of the IGBTs used in a cascade converter. The comparison is based on the efficiency at the nominal point and the power density of the converter. However, according to Beltrame, Sartori and Pinheiro (2016), considering only the efficiency at the nominal point of operation can result in a non-optimized design, depending on the converter operating profile.

The optimal selection of the blocking voltage based on the application mission profile (motor speed and ambient temperature data) and the number of levels are very important for the best performance/cost ratio of the medium-voltage electric drive system. Therefore, this master thesis proposes a methodology to select the optimal blocking voltage of the IGBTs, used in MMC based electrical drives, considering redundancy strategies to achieve the same level of reliability for IGBTs with different voltage classes. In addition, the most suitable design selection is based on the electric drive industrial profile. Thus, the comparison between different designs adopts the complexity of the system, silicon area, efficiency and volume as figures of merit.

The case study is based on a 13.8 kV - 16 MW three-phase induction motor which drives an industrial blower. The mission profile data is obtained from a steel industry in southeastern Brazil. The following contributions are provided:

- Development of a systematic methodology for optimal design for a MMC-based electric drive system;
- Selection of the most suitable design based on the mission profile application, considering the system complexity, performance, cost and energy losses.

The present research has been developed in the Centro Federal de Educação Tecnológica de Minas Gerais (CEFET-MG) in cooperation with the Gerência de Especialistas em Sistemas Elétricos de Potência (GESEP-UFV).

1.3 Organization

This master thesis is organized in 6 chapters as follows. Chapter 1 presents the motivations and objectives of the present master thesis. The electric drives overview is shown in Chapter 2. The MMC-based electric drive system and the control strategies are presented in Chapter 3. In addition the parameter design of the system is presented in this chapter. Chapter 4 presents the case study and the parameters of the MMC-based electric drive system. Furthermore, the figures of merit used for selection of the optimal design are presented in this chapter. The obtained results and discussion are presented in Chapter 5. Finally, Chapter 6 draws the conclusions of this master thesis.

1.4 List of Publications

1.4.1 Published Journal Papers

- P. R. M. Júnior, A. F. Cupertino, G. A. Mendonça and H. A. Pereira, On lifetime evaluation of medium-voltage drives based on modular multilevel converter, in IET Electric Power Applications, vol. 13, no. 10, pp. 1453-1461, 10 2019, doi: 10.1049/iet-epa.2018.5897.

- P. R. M. Júnior, J. V. M. Farias, A. F. Cupertino, H. A. Pereira, M. M. Stopa and J. T. de Resende, Redundancy and Derating Strategies for Modular Multilevel Converter for an Electric Drive, in Jornal of Control, Automation and Electrical Systems, 31, 339–349 (2020), https://doi.org/10.1007/s40313-019-00537-z.

- P. R. M. Júnior, J. V. M. Farias, A. F. Cupertino, G. A. Mendonça, M. M. Stopa, H. A. Pereira, Seleção da Tensão de Bloqueio Ótima de IGBTs para Inversores de Frequência Baseados em Conversor Modular Multinível, in Revista Eletrônica de Potência - SOBRAEP, v.25, n. 4, dec. 2020, http://dx.doi.org/10.18618/REP.2020.4.0033.

1.4.2 Published Conference Papers

- P. R. M. Júnior, J. V. M. Farias, A. F. Cupertino, G. A. Mendonça, M. M. Stopa and H. A. Pereira, Selection of the Number of Levels of a Modular Multilevel Converter for an Electric Drive, 2019 IEEE 15th Brazilian Power Electronics Conference and 5th IEEE Southern Power Electronics Conference (COBEP/SPEC), Santos, Brazil, 2019, pp. 1-6, doi: 10.1109/COBEP/SPEC44138.2019.9065903.

2 State of Art

2.1 Introduction

Power electronic converters currently play a very important role in numerous applications and are one of the key solutions increasing the efficiency of modern drive systems. A structural overview of the main medium-voltage drive topologies is presented in Fig. 4. The medium-voltage high-power converter can be classified into direct and indirect converter topologies. In addiction, the indirect topologies can be grouped into two main categories: current source converters (CSC) and voltage source converters (VSC).

This chapter provides a literature overview on power converter topologies. The main characteristics, challenges and applications of each family will be presented. In addition, an analysis of the converters available on the market is also shown.

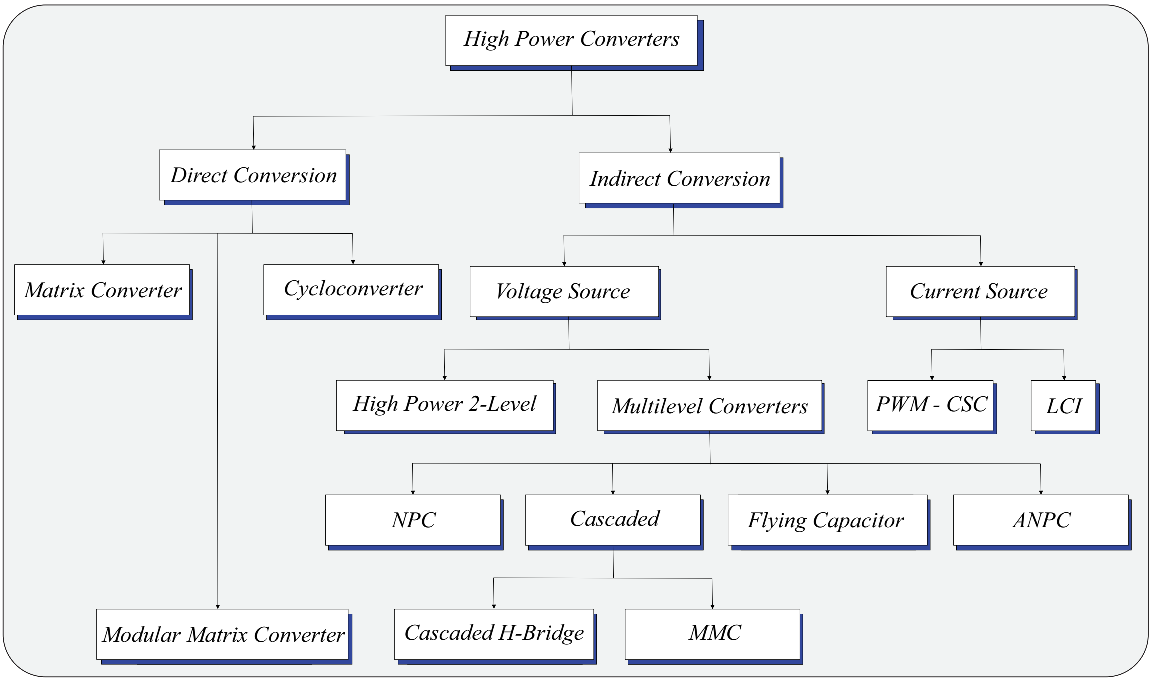

Figure 4 – Structural overview of medium-voltage drives topologies.

2.2 Electric Drives Overview

For the direct converters, the cycloconverter (CCV) is the most used topology in high-power applications. CCV converts a three-phase ac voltage with a fixed magnitude and frequency to a three-phase ac voltage with variable magnitude and frequency (Wu et al., 2008). The technique of cycloconversion was known in the 1930's, when mercury-arc rectifier were used to supply railway transportation systems (Rissik, 1935). After the development of thyristors in the late of 1950's, the new cycloconverter were applied to variable-frequency induction motor drive (Slabiak; Lawson, 1966). The CCV are based on the anti-parallel connection of thyristor bridges without a dc link, as described on Fig. 5. The main advantages of thyristors based converters are the low switching losses, the bidirectional power flow, very high-power ratings and simple and robust structure. On the other hand, the drawbacks are the limited frequency range, low power factor at low motor speed and low power quality (Wu et al., 2008; Hiller; Sommer; Beuermann, 2010; Kouro et al., 2012). The main applications of the CCV is in high-power drives for control in low speeds, such as rolling mills, cement mills, ore grinding mills, ship propulsion and mine winders (Stemmler, 1994; Kouro et al., 2012).

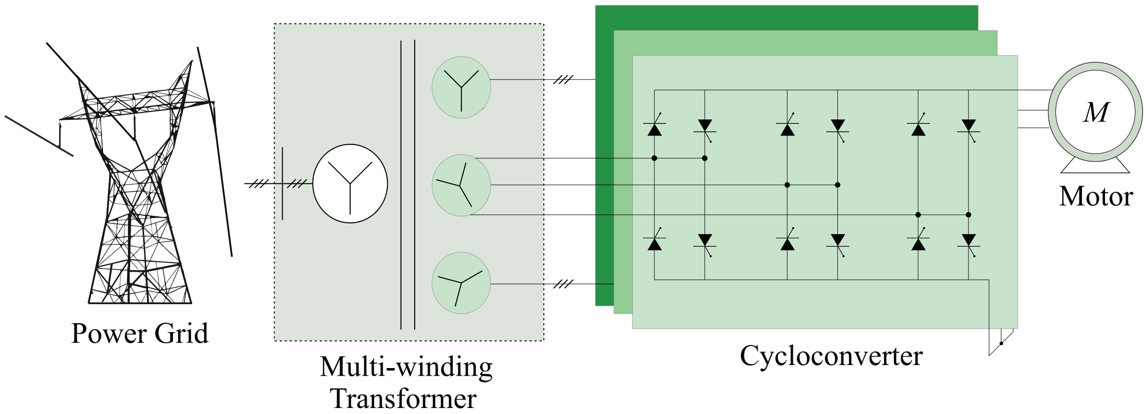

Figure 5 – Schematic of the three-phase CCV.

Another direct converter topology is the matrix converter (MC). This topology was developed in the 1960s (Gyugyi; Pelly, 1969). However, significant improvements in topology were introduced only in the 1980s (Alesina; Venturini, 1989). The MC connects the input ac lines to the output ac lines through bidirectional switches without need of energy storage devices, as shown in Fig. 6. The switches are controlled in such a

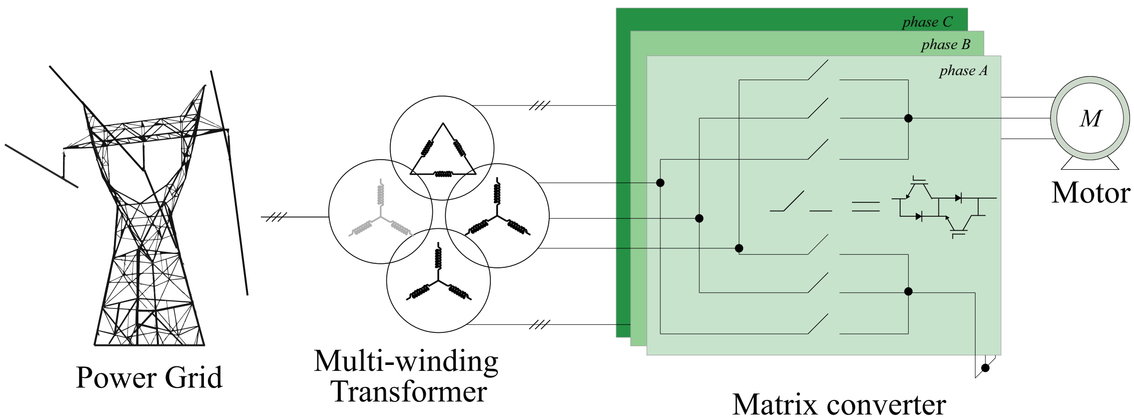

Figure 6 – Schematic of the three-phase MC.

way that the average output voltage is a sinusoidal waveform of the desired frequency and amplitude. The main advantages are the lack of energy storage devices and smaller footprint. Therefore, this topology is useful for high-power drives where limited space is available, such as pumps in ships and rigs and aerospace applications (Kouro et al., 2012; Munuswamy; Wheeler, 2019). Among the disadvantages are the great number of semiconductors needed, special consideration for modulation to avoid forbidden switching states in the bidirectional switches, output voltage capability and harmonic mitigation (Chai et al., 2016; Nguyen; Lee, 2016; ABB, 2019).

Finally, modular matrix converter developed by (Erickson; Al-Naseem, 2001) in the 2000s is a direct and also multilevel converter. This converter consists of three subconverters and nine clusters, as shown in Fig. 7. This topology enables the direct ac-ac bidirectional power flow and low distortions in the input/output currents (Kawamura et al., 2015). In addiction, the modular matrix converter has shown some advantages in applications that requires high-torque at low speeds, such as mills, kilns, conveyors and extruders (Okazaki et al., 2015; Akagi, 2017; Okazaki et al., 2017; Diaz et al., 2020). Among the disadvantages are the high capacitors voltage ripples when the motor operates close to the line frequency (Okazaki et al., 2017). No company has commercialized medium-voltage motor drives using modular matrix converters due to some reasons, including cost and complexity. However,

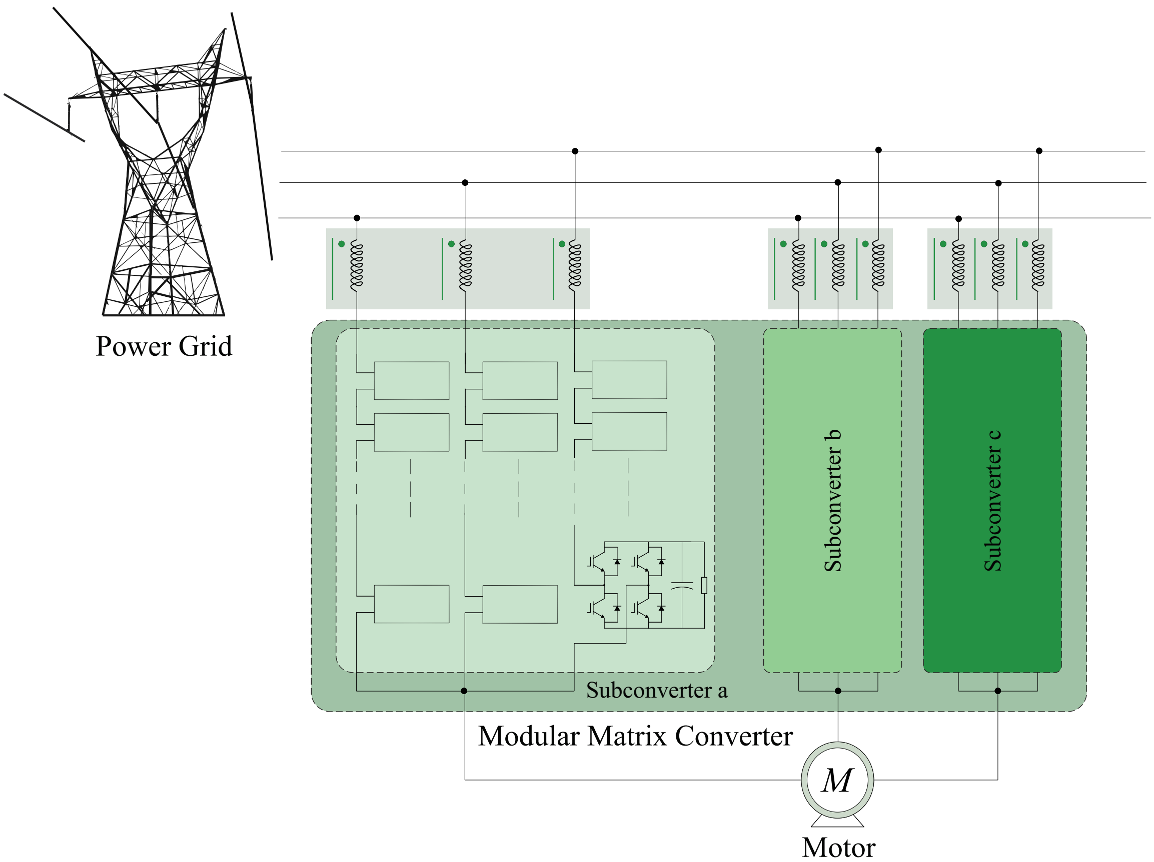

Figure 7 – Schematic of the three-phase modular matrix converter.

some authors expect that traditional cycloconverters will be replaced with the modular matrix converters in the near future (Akagi, 2017; Diaz et al., 2020).

On the indirect conversion topologies, the CSCs technologies are suited for high-power applications. The main features of CSC include a simple structure, low number of devices, low dv/dt , high reliability, and over current and short-circuit protection, unlike VSCs. Despite all of these advantages, it has a limited dynamic performance because of the large dc inductor used in the dc-link (Wu et al., 2008; Kouro et al., 2012). The CSCs are classified into load-commutated inverter (LCI) and pulse-width modulated current source inverter (PWM-CSI).

The LCI is one of the earliest topologies used in the high-power variable speed drives, in the 1980s (Abbondanti, 1989). This converter is based controlled rectifier and SCR inverter, as shown in Fig. 8. The controlled thyristor rectifier is used to adjust the magnitude of dc link current smoothed by an inductor (Kouro et al., 2012). The thyristor devices do not have the self-turn-off capability. The LCI are suitable for very large electric drives with tens of megawatt power capacity, such as power generation and wind tunnels (ABB, 2018). This is due to the use of thyristor devices that lead to a low manufacturing cost and high energy efficiency when compared with IGBT or IGCT devices used in other types of drives (Wu et al., 2008). The main disadvantages are the grid current harmonics, the requirement of additional filters, and the low dynamic performance (Emery; Eugene, 2002; Kouro et al., 2012).

Unlike LCI, the PWM-CSI employs force-commuted devices such as GTO, GCT and IGCT (Hombu; Ueda; Ueda, 1987). This topology found in heavy-duty medium-voltage drives has been a major player in this area. The typical configuration of the PWM-CSI is shown in Fig. 9. The current version of this topology also features an integrated

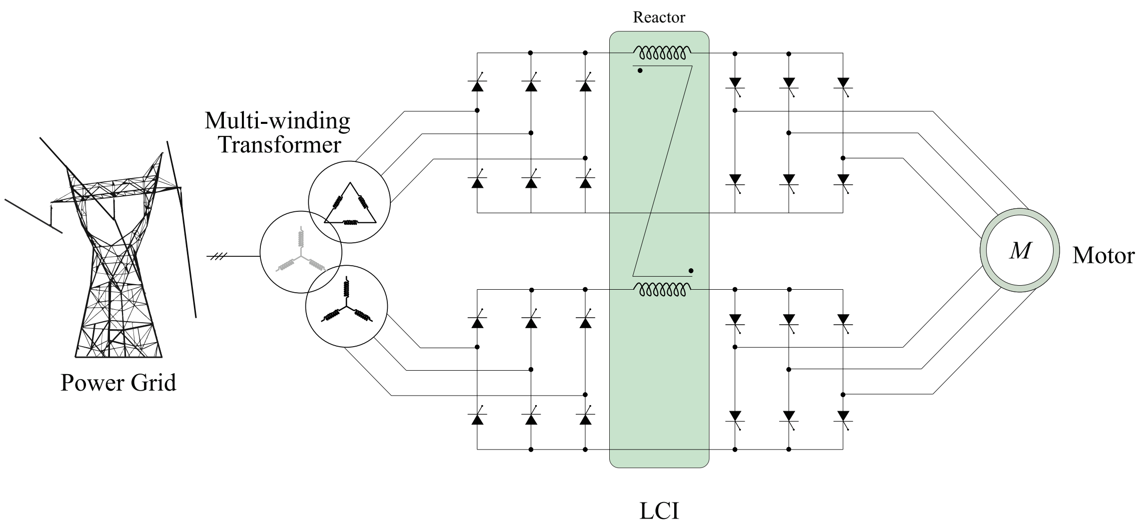

Figure 8 – Schematic of the three-phase LCI.

common-mode dc choke that enables transformerless operation (Wu et al., 2001; Wu et al., 2008). Indeed, the PWM-CSI was the first transformerless medium-voltage drive on the market (Kouro et al., 2012). The main advantages of this topology are the absence of dv/dt, no wave reflection, simple converter structure, transformerless topology, and inherent overcurrent and short-circuit protection. The main disadvantage is the lower dynamic performance due to the large dc choke. This topology is well suited for high-power low dynamic requirements applications, such as pumps, fans, and compressors.

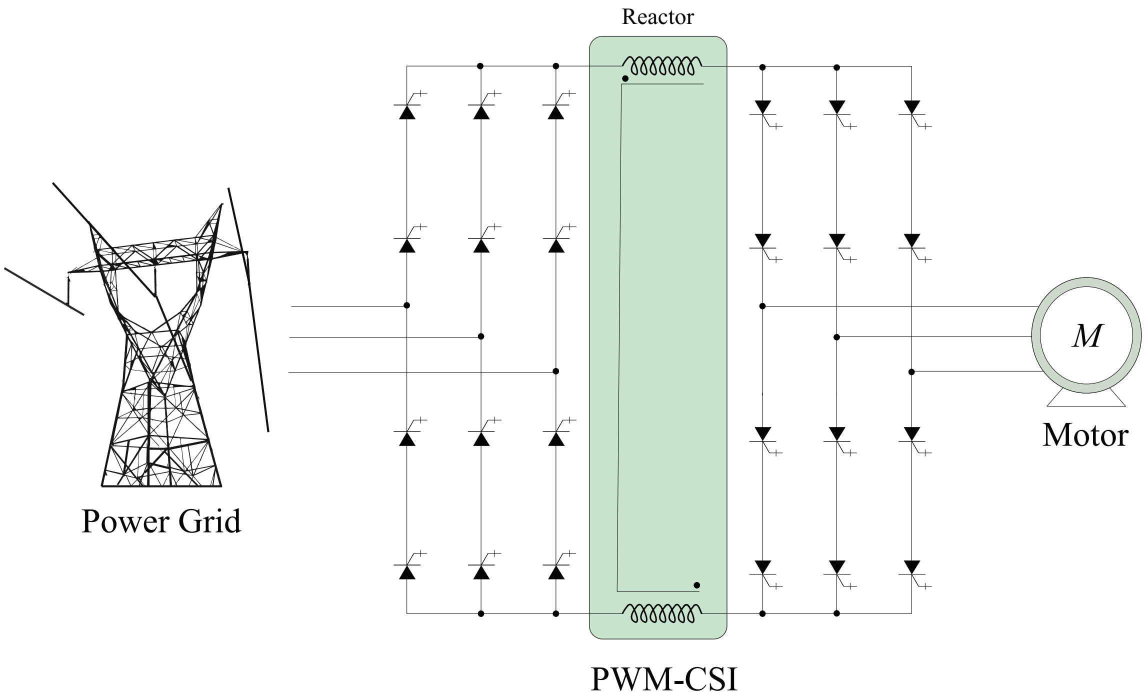

Figure 9 – Schematic of the three-phase PWM-CSI.

About the VSC's, in low-voltage applications, the 2-level voltage source converter (2L-VSC), Fig. 10, is the standard converter topology for dc-ac conversion since the 1960s (Mcmurray, 1965), due to its simple topology, low number of installed components, robustness and straighforward control. Although the application of electric drives is generally advantageous, it leads to several issues, such as (Kerkman; Leggate; Skibinski, 1996; Busse et al., 1997; Wheeler, 2005):

- high harmonic content cause additional losses in the motor;
- the high dv/dt cause premature failure of the motor insulation, bearing problems, electromagnetic emission and wave reflection;
- the CM voltage leads to premature failure of the motor winding;
- low number of levels in the output voltage causes torque vibrations in the motor shaft.

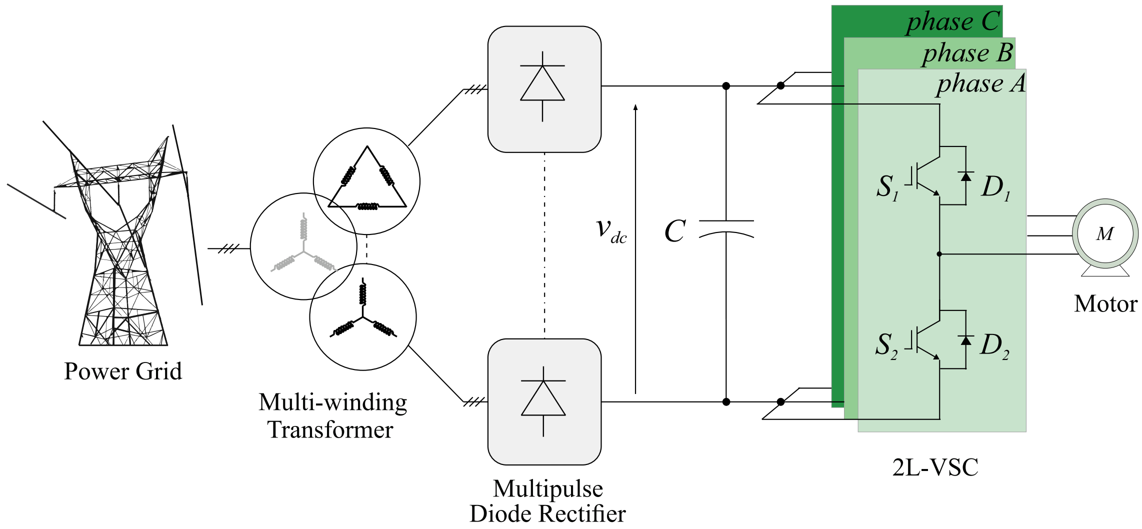

Figure 10 – Schematic of the three-phase 2L-VSC.

Further challenges arise when 2L-VSC are employed in medium-voltage electric drives. There are two options that increase the achievable voltages of the converter. The first option is to use semiconductors with higher blocking voltages, such as high-voltage IGBTs. However, the maximum blocking voltage of the currently available silicon-based semiconductor IGBTs is limited to 6.5 kV. Additionally, these switches are significantly more costly than the standard low-voltage IGBTS. The second option is to increase the converter's voltage, stacking multiple identical semiconductor switches in series as shown in Fig. 11. Nevertheless, this solution is very complex due to some practical issues, such as voltage and losses equalization between the series devices (Shammas; Withanage; Chamund, 2006; Fortes; Mendes; Cortizo, 2019). Finally, if the semiconductor switches are stacked in

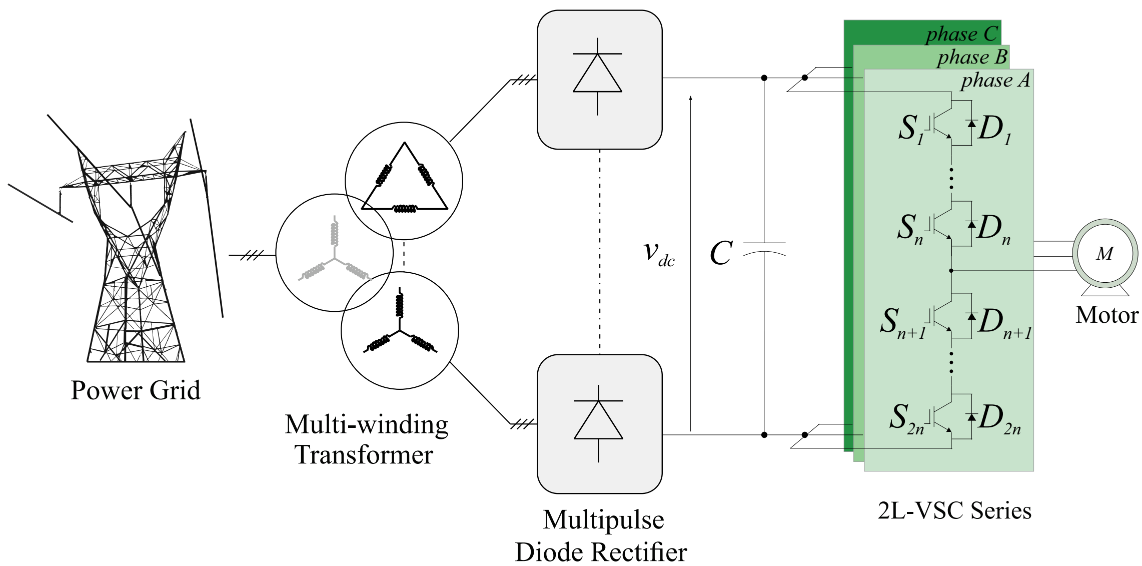

Figure 11 – Schematic of the three-phase 2L-VSC with series connection of semiconductor devices.

series, their dv/dt is summed, massively increasing the significance of long-cable reflection and bearing current problems for an application in medium-voltage drives. Thus, this topology has been discontinued (although some drives commissioned in the last decade are still operative) (Kouro et al., 2012).

A solution for medium-voltage drives that reduces the height of voltage steps at the converter output, and thus also the dv/dt and the voltage harmonics, was introduced with multilevel converters in the 1970s (Mcmurray, 1971). This converter concept allows the use of lower voltage semiconductors to achieve higher voltages (Franquelo et al., 2008).

The neutral point clamped (NPC) (Nabae; Takahashi; Akagi, 1981) was the first multilevel converter employed in large scale. The three-level NPC (3L-NPC) is the NPC topology most used in the medium-voltage drives industry. This topology uses an arrangement of four power switches per leg, clamped with diodes to a midpoint of the dc-link, as shown in Fig. 12. In this way, each switch blocks half of the total dc-link voltage, enabling medium-voltage operation with IGBT devices. In addition, the converter can clamp the phase output to the neutral point, generating an extra voltage level compared with 2L-VSC. This results in a reduction of dv/dt and improved power quality, which made the 3L-NPC an interesting solution for medium-voltage drives (Kouro et al., 2012). In general, the 3L-NPC is characterized by a relatively small dc-link capacitance, simple power circuit topology, low component count, straightforward protection and modulation schemes (Diab, 2019).

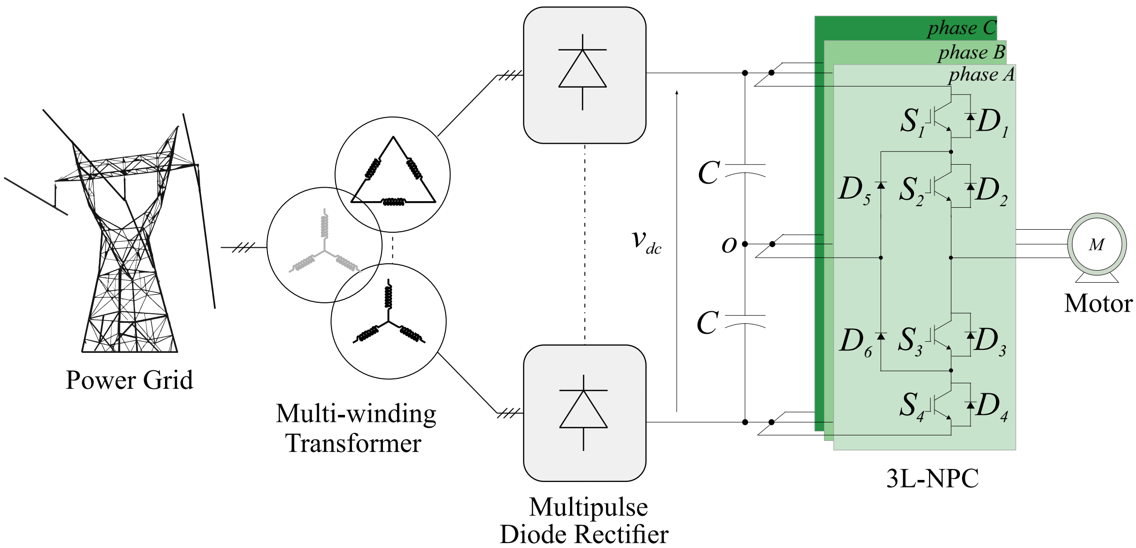

Figure 12 – Schematic of the three-phase 3L-NPC.

One of the disadvantages of 3L-NPC is that the power switches do not have symmetric losses, forcing a derating of the devices or use of different switches (Bruckner; Bernet; Guldner, 2005; Ma; Blaabjerg, 2016). Moreover, this topology has a limited number of voltage levels for practical applications, because it requires a series connection of diodes and auxiliary balancing circuits to balance the capacitor voltages (Busquets-Monge et al., 2008). An alternative NPC topology to solve this inherent issue, which avoids series association of the clamping diodes was proposed in (Xiaoming Yuan; Barbi, 2000). Due to the increasing complexity of the control for the balancing of the dc-link capacitors and the physical construction with an increasing number of levels, the NPC topologies available in the markets are limited to five-level NPC (5L-NPC) (Abu-Rub et al., 2010; Akagi, 2017). The typical applications for these topology are pumps, fans and conveyors, rolling mills and railway traction systems (Kouro et al., 2012).

To solve the problem of thermal unbalance of the devices, the active neutral point clamped converter (ANPC) was developed (Bruckner; Bernet, 2001) in the 2000s. In this topology, the clamping diodes are replaced by clamping switches as shown in Fig 13. This arrangement provides a controllable path for the neutral current and hence control the loss distribution among the switches of the converter (Bruckner; Bernet; Guldner, 2005). As a consequence, higher power ratings and switching frequencies are possible. However, as the NPC, the ANPC converter has a limited number of voltage levels for practical applications. This has been used to successfully control the rotor currents of a 200-MVA doubly fed induction machine for a hydro pumped storage system (Kouro et al., 2012).

A further topology is the flying capacitor multilevel converter (FCMC), introduced by (Dickerson; Ottaway, 1971) in the 1970s. However, was improved for medium-voltage drives in the 1990s (Meynard; Foch, 1992). The three-level FCMC (3L-FCMC) is shown in Fig. 14. The converter generates additional voltage levels, while reducing the voltage stress on the power switches, by clamping capacitors between two devices. Additional switches and capacitors can be connected, increasing the number of voltage levels of the converter, and it is considered a modular structure. However, the number of voltage levels of FCMC

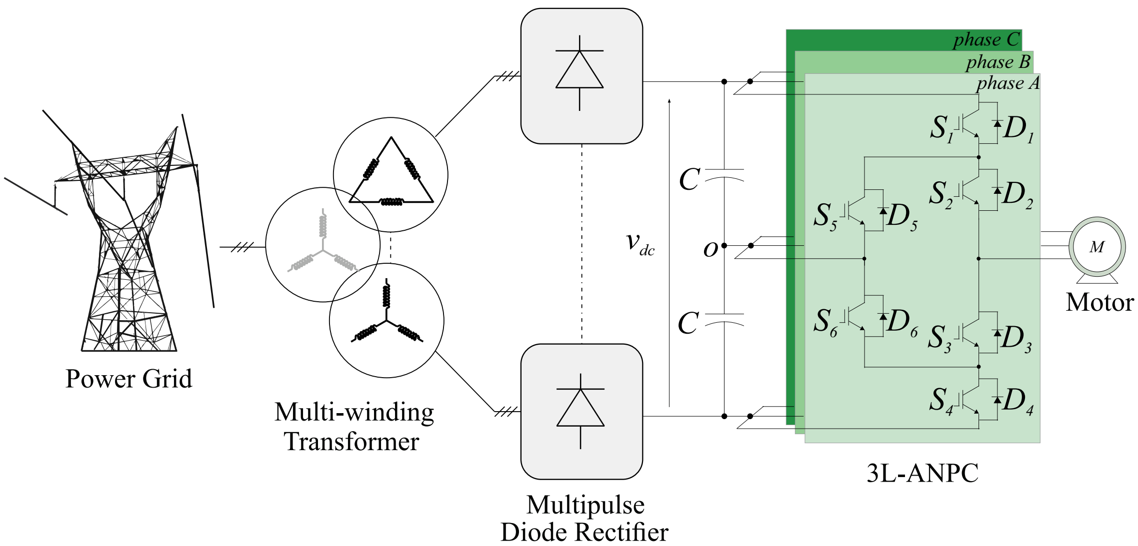

Figure 13 – Schematic of the three-phase 3L-ANPC.

is limited in commercial applications, since each flying capacitor within the converter has to be designed for different requirements, and the balancing of the flying capacitors becomes more complex with the increasing number of levels (Abu-Rub et al., 2010; Akagi, 2017). Furthermore, the switching frequencies of the converter have to be relatively high to reduce the capacitances of flying capacitors (Rodriguez et al., 2007; Abu-Rub et al., 2010). The main applications of the FCMC are train traction drives and pumps in the water industry (Kouro et al., 2012).

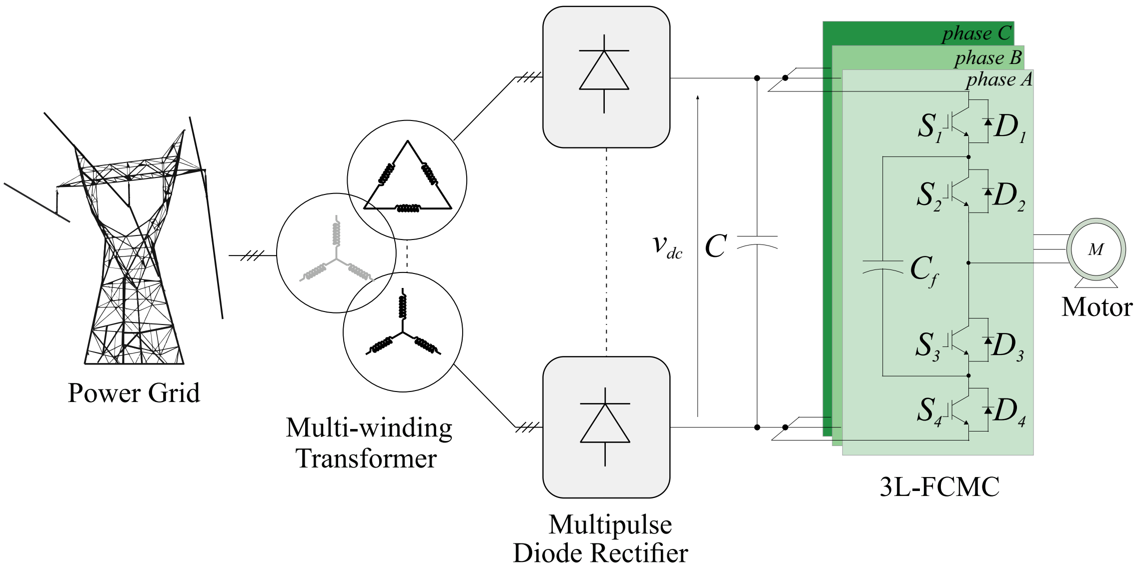

Figure 14 – Schematic of the three-phase 3L-FCMC.

The first multilevel converter linearly scalable in voltage was the cascaded H-bridge (CHB) converter introduced by the company "Robicon", part of Siemens, and it is currently a popular solution for medium-voltage drives since the 1990s (Hammond, 1997). The converter topology is shown in Fig 15. The converter is based on series-connected modules, which are individually supplied by a zig-zag transformer. The phase shifts between the individual transformer windings are chosen to cancel the low-frequency grid harmonics caused by the diode rectifiers (Hammond, 1997). Since the modules are cascaded, the number of voltage levels can be increased linearly. The main drawback and limiting factor of this topology is the bulky and zig-zag transformer, which must be redesigned for each number of levels (Malinowski et al., 2010). In addiction, this transformer tends to be expensive and inefficient, rendering the converter bulky and heavy (can produce about 50% of the total power losses, occupy up to 50% of the system space and represents up 70% of the system weight) (Fang Zheng Peng et al., 1995; Hagiwara; Akagi, 2009; Abu-Rub et al., 2016). The main applications of the CHB are pumps in the water industry and fans in the cement industry (Kouro et al., 2012).

A solution for dc-ac conversion, omitting the requirement of the bulky multi-winding transformer, consequently isolated dc-sources, was introduced with the Modular Multilevel

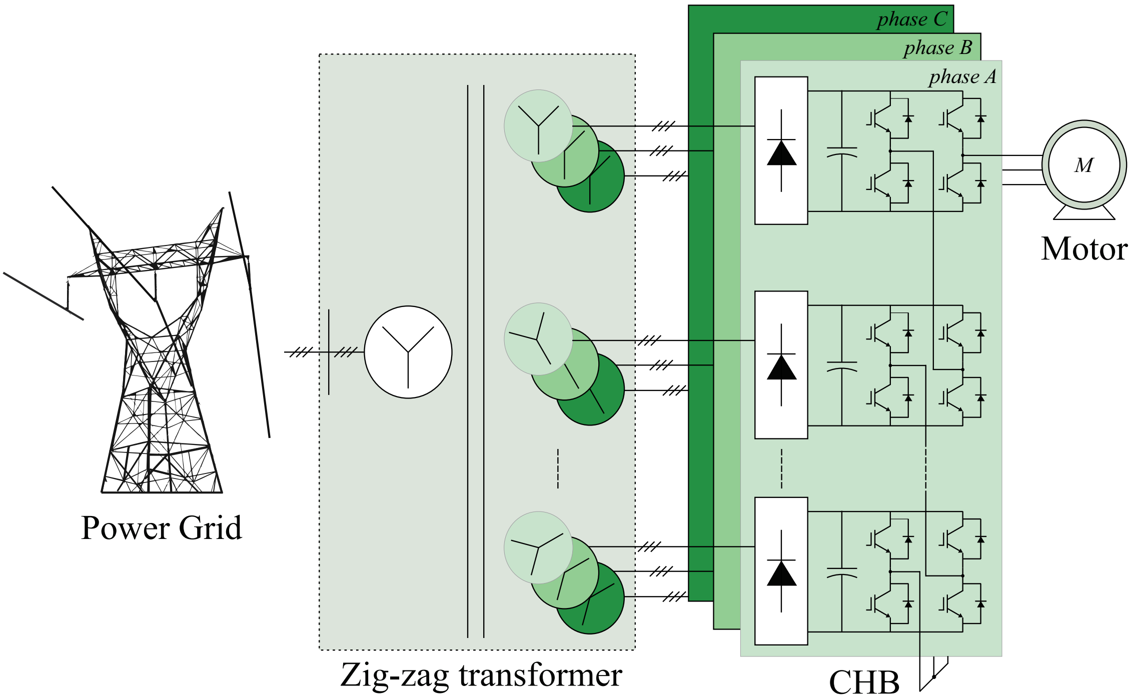

Figure 15 – Schematic of the three-phase CHB.

Converter (MMC) (Marquadt, 2001; Lesnicar; Marquardt, 2003). Basically, the MMC is composed of single-phase low-voltage converters, called submodules (SM), connected in series in each of the six converter arms, as shown in Fig. 16. The SM can have a number of different designs. Originally, MMC was proposed with half-bridge (HB) and full-bridge (FB) cells. The main advantage of half-bridge SM is the cost. However, this structure cannot handle dc-link short circuits, which is an important concern in high-voltage direct current (HVDC) systems. In spite of HVDC systems, in electric drive applications the probability of short-circuit in dc-link can be reduced considerably by an adequate design of the converter bus bars. In this context, half-bridge SM can be employed.

Because the modular construction, this topology provides superior voltage scalability. In addition, low switching frequencies can be employed, which leads to high efficiency. Therefore, MMC has become a preferred solution for HVDC applications and is commercialized by several companies. For the medium-voltage electric drives field, the MMC presents several properties that are very advantageous, such as (Kouro et al., 2010; Hagiwara; Hasegawa; Akagi, 2013; Antonopoulos et al., 2014; Pan et al., 2020):

- high number of voltage levels, leading to small voltage steps;
- inherent redundancy and fault-tolerance structure;
- scalability, modularity and flexibility, the voltage rating can be increased by installing more SMs;

- low switching frequency, leading to a high efficiency;
- there is no need for high-voltage dc-link capacitors (or series connected) since the intrinsic capacitors of the SMs perform these tasks.

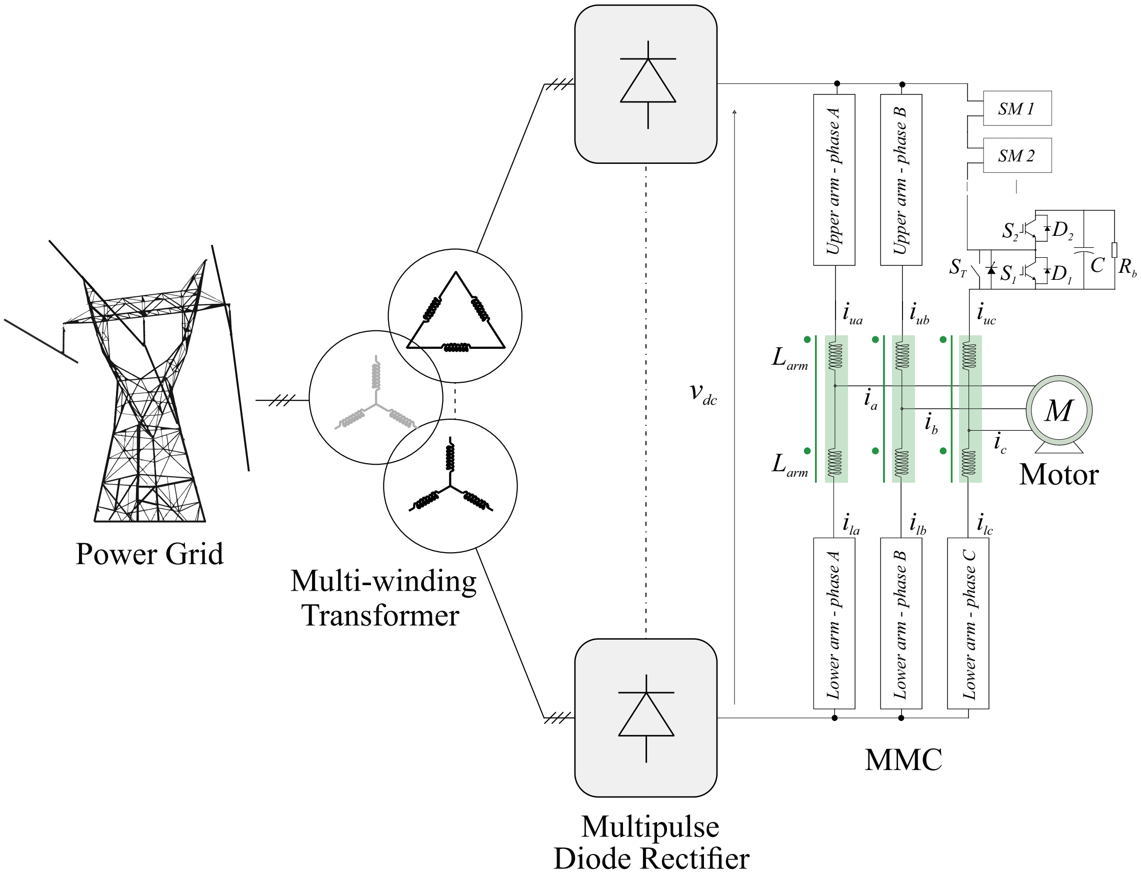

Figure 16 – Schematic of the three-phase MMC.

About MMC topologies, the MMC based on half-bridge SMs is widely used in electric drives which load torque is a quadratic function of the motor speed (Akagi, 2017). This type of load is easily found in the industrial field, accounting for approximately 70% of the market for medium-voltage electrical drives, as shown in Fig. 1 (Wu; Narimani, 2017). However, this topology has some limitations in electrical drive application, mainly for low speed high-torque operation (Hagiwara; Hasegawa; Akagi, 2013). In order to improve the MMC dynamics at low speeds, it is necessary to use some techniques to mitigate the voltage ripple of the SM capacitors (Hagiwara; Hasegawa; Akagi, 2013; Antonopoulos et al., 2014; Li et al., 2017; Kumar; Poddar, 2017; Kumar; Poddar, 2018). Companies like Siemens and Benshaw solved this problem and already have this converter topology in the market for pumps, blowers and compressors (Hagiwara; Nishimura; Akagi, 2010; Akagi, 2017; Li et al., 2017; Dekka et al., 2017; Benshaw, 2018; Siemens, 2018).

Table 2 provides a summary of the medium-voltage drive products offered by major drive manufacturers in the world, where the inverter configuration, and power range of the drive are listed. Different multilevel topologies, NPC, ANPC, FCMC, CHB and MMC are examined. It is evident that multilevel converters have been widely used among industrial companies. Among the conventional topologies, NPC is the most adopted one for the medium-voltage electrical drives, while the CHB is the second most adopted. For the relatively new multilevel topologies, the MMC-based medium-voltage electric drive is commercialized only by Siemens and Benshaw.

Table 2 – Market overview of medium-voltage drives.

Topology	**Trade Mark**	**Power Range**	**Voltage Range**	**Manufacturer**
CCV	CL9000	5 - 100 MVA	1 - 5 kV	Alstom
CCV	Sinamics SL150	12 - 40 MVA	1.5 - 4 kV	Siemens
MC	FSDrive-MX1S	0.32 - 5 MVA	3 - 6 kV	Yaskawa
CSI	CDM8000	8.3 - 13.5 MVA	6 - 10 kV	Alstom
CSI	PowerFlex 7000	0.15 - 6.3 MVA	2.3 - 6.6 kV	Rockwell
LCI	MEGADRIVE-LCI	2 - 150 MVA	2 - 25 kV	ABB
LCI	SD7000	3 - 100 MVA	1.5 - 15.75 kV	GE
LCI	Sinamics GL150	6 - 85 MVA	1.4 - 10.3 kV	Siemens
2L-VSC	VDM 5000	0.3 - 5 MVA	2.3 - 4.2 kV	Alstom
NPC	VDM 7000	7 - 9.5 MVA	3.3 kV	Alstom
NPC	ACS 1000/5000/6000/6080	1.4 - 36 MVA	2.3 - 13.8 kV	ABB
NPC	VACON 3000	2.2 - 7 MVA	3.3 - 4.16 kV	Danfoss
NPC	SC 9000	0.22 - 9 MVA	2.4 - 13.8 kV	Eaton
NPC	MV 7000	3 - 81 MVA	3.3 - 13.8 kV	GE
NPC	Ingedrive MV100/500/900	0.8 - 44 MVA	3.1 - 6.6 kV	Ingeteam
NPC	Altivar 1260	0.5 - 5 MVA	4.16 kV	Schneider
NPC	Sinamics GM150/SM150	2 - 31.5 MVA	2.3 - 4.16 kV	Siemens
NPC	Dura-Bilt5i MV	0.15 - 7.5 MVA	2.3 - 4.16 kV	TMEIC
NPC	T300MV/T300BMV2/MTX2	0.23 - 8.2 MVA	2.4 - 4.16 kV	Toshiba
NPC	MVW01	0.4 - 36 MVA	2.3 - 6.9 kV	WEG
ANPC	ACS 2000	0.3 - 3.6 MVA	4.16 - 6.9 kV	ABB
ANPC	PCS 8000	6 - 100 MVA	6 - 13.8 kV	ABB
FCMC	VDM 6000	2.2 - 8 MVA	2.3 - 4.2 kV	Alstom
CHB	ACS 580MV	0.2 - 6.3 MVA	6 - 11 kV	ABB
CHB	AXPERT-HIVERT	0.25 - 12.5 MVA	3.3 - 11 kV	Amtech
CHB	MVD 1000/2000/3000	0.16 - 12.8 MVA	3.3 - 11 kV	Delta
CHB	FRENIC4600	0.3 - 18.3 MVA	3 - 11 kV	Fuji
CHB	HIVECTOLHVI-E	0.3 - 14.7 MVA	3.3 - 11 kV	Itachi
CHB	Harvertst A/S/VA	0.25 - 6.25 MVA	3 - 11 kV	Harverst
CHB	LSMV - M1000	0.2 - 12.5 MVA	3 - 11 kV	LS Electronic
CHB	PowerFlex 6000	0.15 - 11 MVA	2.3 - 11 kV	Rockwell
CHB	MVC	0.6 - 10 MVA	3 - 10 kV	Rongxin Power
CHB	Altivar ATV6000	3.5 - 5.8 MVA	4.16 - 6.6 kV	Schneider
CHB	Sinamics GH180	3.5 - 24.4 MVA	2.3 - 11 kV	Siemens
CHB	MVW3000	0.13 - 12.1 MVA	1.15 - 13.8 kV	WEG
CHB	MV 1000	0.13 - 12 MVA	2.4 - 11 kV	Yaskawa
MMC	M2L	0.22 - 9 MVA	2.3 - 7.2 kV	Benshaw
MMC	Sinamics GH150	4 - 48 MVA	4.16 - 13.8 kV	Siemens

2.3 Chapter Conclusions

In this chapter, a detailed review of the main power converter topologies widespread in the literature was presented. Direct conversion converters, current source converters and voltage source converters were discussed. In addition, market research was carried out with the main manufacturers of power converters and their respective models and characteristics. Among the topologies, the MMC presents interesting characteristics for the applications of pumps, fans and blowers. Such characteristics and application sector make it a very attractive and promising topology for medium voltage electric drive applications with high efficiency and reliability.

The next chapter present the topology of MMC-based electric drive. In addition, the control schemes and the CMI employed were discussed. Furthermore, the design of the main components and variables were presented. Finally, some redundancy strategies and the reliability study were also presented in this chapter.

3 MMC-based Electric Drive System

This chapter aims to present the topology and characteristics of MMC-based electric drive system. Then, the control scheme and the strategy to reduce the voltage ripple of the capacitors when the motor operates at low speed are described. Furthermore, the design of the main components and variables were presented. Five designs of MMC with best utilization factor for each blocking voltage are selected for furthers comparisons. Finally, some redundancy strategies and the reliability study are presented in this chapter.

3.1 Topology

The structure of the MMC-based electric drive system is shown in Fig. 17. As observed, this topology is based on cascade association of half-bridge cells, generally consisting of two IGBTs, S_1 and S_2, two diodes, D_1 and D_2, and a SM capacitor, C. A bypass switch S_T is usually installed in parallel with each SM. This device has the purpose of bypassing it if any fault is detected (Gemmell et al., 2008; Farias et al., 2018). Thus, the topology becomes inherently fault tolerant. Unlike the CHB-based drives, this topology features a single dc power supply, similarly to a 2-level inverter or NPC. Therefore, the complex zig-zag transformer can be eliminated. The MMC has N effective and M redundant SMs per arm. R_b represents the bleeder resistor. The arm inductors L_{arm} reduce the harmonic distortion in the circulating currents (Harnefors et al., 2013; Farias et al., 2018).

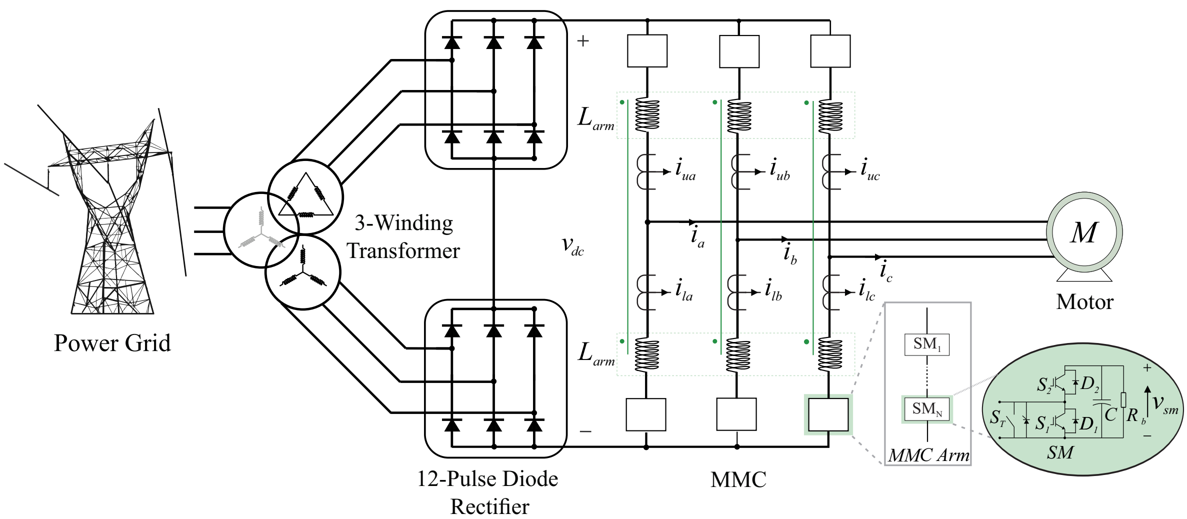

Figure 17 – Three-phase MMC-based electric drive system.

3.2 Control Structure

Regarding the control scheme, the strategy is based on (Hagiwara; Hasegawa; Akagi, 2013) and the control structure is presented in Fig. 18. The control structure can be divided into:

- MMC averaging control: averaging voltage loop and circulating current loop to perform the energy balance between the phases and minimize the value of the circulating current;
- MMC balancing control: individual balancing control for balancing each capacitors voltage;
- motor control: rotor field oriented control (RFOC) performed by controlling the output current of the converter.

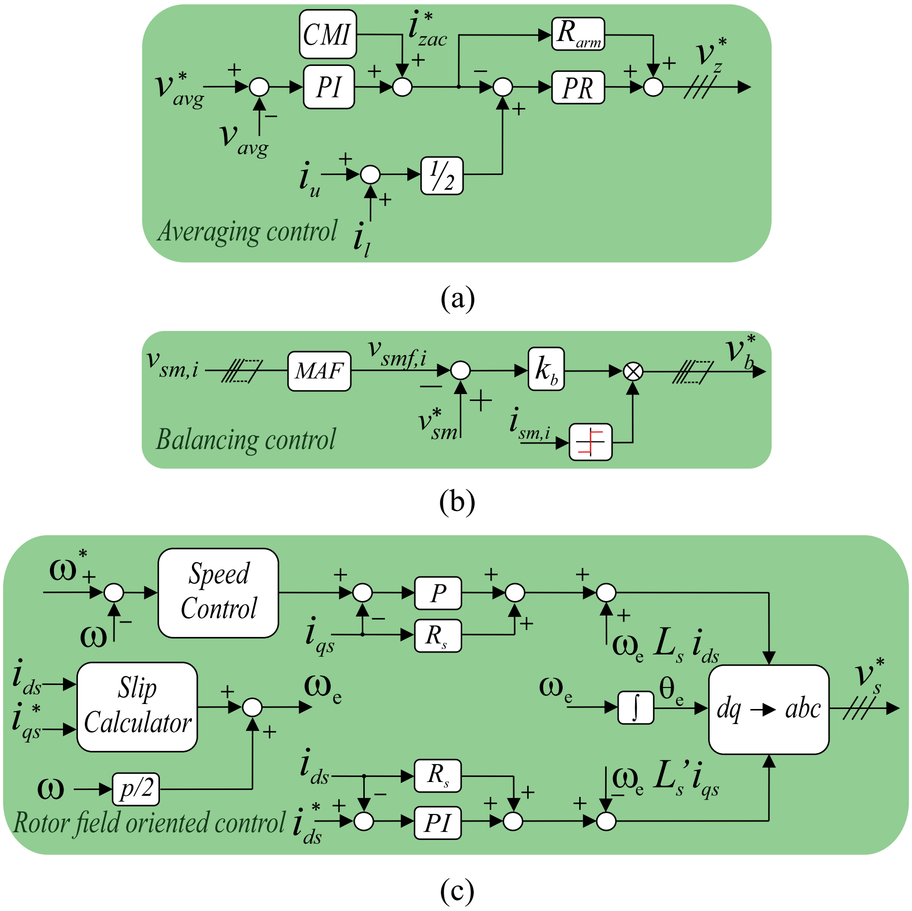

Figure 18 – Control scheme for MMC based electric drive system: (a) Average and circulating current control; (b) Individual balancing control; (c) Rotor field oriented control. CMI - Common-mode injection. MAF - Moving average filter.

The averaging voltage control and circulating current control is shown in Fig. 18 (a). The external loop controls the average voltage v_{avg} of all SMs per phase. This average voltage is computed by:

$$v_{avg} = \frac{1}{N_T} \sum_{i=1}^{N_T} v_{sm,i}, \tag{3.1}$$

where $v_{sm,i}$ is the ith SM voltage per phase. N_T is the total number of operating SMs per phase, given by:

$$N_T = N_{o,u} + N_{o,l}, \tag{3.2}$$

where $N_{o,u}$ and $N_{o,l}$ are the number of operating SMs of the upper and lower arms, respectively.

The average voltage calculates the necessary circulating current to the inverter leg. This control also manages the energy exchange among the converter arms. The inner loop is responsible for controlling the circulating current to mitigate the harmonics in the circulating current and introduces damping in the converter dynamics. This control is based on proportional resonant (PR) controller, to suppress the second harmonic component, which is a common issue in modular multilevel converters (Xu et al., 2016; Farias et al., 2018).

As a notable drawback, MMC presents high voltage ripple in the SM capacitor voltages when the motor is operating at low-frequency range. This fact is observed, since the capacitors voltage ripple is approximately inversely proportional to the stator motor frequency (Hagiwara; Nishimura; Akagi, 2010):

$$\Delta v_{sm} \approx \frac{\sqrt{2} I_s}{4\pi f_s C}, \tag{3.3}$$

where I_s is the stator rms current and f_s is the frequency of the voltage applied in the motor. Thus, large oscillations in the capacitor voltages occur during the motor start-up, which results in control instabilities and large stresses in the SM capacitors (Antonopoulos et al., 2014).

In order to reduce the capacitor voltage ripple under low speeds, a common-mode injection (CMI) is employed. This strategy consists of inserting an alternating circulating current and a common-mode voltage in the reference signals. This concept was firstly proposed by (Korn; Winkelnkemper; Steimer, 2010). As shown in this reference, the higher the common-mode voltage injected, the lower the required circulating current amplitude. This is very important, since the circulating current affect the converter power losses (Korn; Winkelnkemper; Steimer, 2010). Hagiwara, Hasegawa and Akagi (2013) employs the sinusoidal signal added to a third-order harmonic ripple mitigation technique. This strategy is employed in the present Thesis. This method consists of inserting a common-mode voltage, v^*_{com}, and circulating current, i^*_{zac}, which reduces the capacitors ripple. The v^*_{com} and i^*_{zac} are given by:

$$v^*_{com} = -\sqrt{2}V^*_{com}(\sin(\omega_{com}t) + 0.16\sin(3\omega_{com}t)), \tag{3.4}$$

$$i^*_{zac} = \frac{1}{\sqrt{2}V^*_{com}}\left(\frac{2v^{*2}_s}{v_{dc}} - \frac{v_{dc}}{2}\right) i_s(\sin(\omega_{com}t) + 0.16\sin(3\omega_{com}t)) + \frac{v^*_s i_s}{v_{dc}}, \tag{3.5}$$

where V^*_{com} is the rms value of v^*_{com}. The common-mode voltage angular frequency is represented by ω_{com} (=$2\pi f_{com}$). The common-mode frequency, f_{com}, used is 54 Hz and the amplitude of the third harmonic inserted is 1/6 of the fundamental component (Hagiwara; Hasegawa; Akagi, 2013). v^*_s is the stator reference voltage computed by RFOC and i_s is the stator current. Moreover, the CMI is employed at the 0 to 20 Hz range, where it has the greatest impact on the voltage ripple, as suggested in (Hagiwara; Hasegawa; Akagi, 2013). It is important to highlight that the amplitude of the common-mode voltage is limited by the converter modulation index. Therefore, this strategy is suitable for mechanical loads which does not require high torque at low speed range, e.g. blower-like loads.

Furthermore, the individual balancing control is used to guarantee that the individual capacitor voltage is balanced according to the reference value (Debnath et al., 2015). For this strategy, the individual control is composed of a proportional controller, as shown in Fig. 18 (b). The moving average filter (MAF) attenuates the capacitor voltage ripple and to improve the individual balancing performance. Then, its output is multiplied by the arm current. The obtained signal is added to the modulator reference signal.

Finally, the last control structure is shown in Fig. 18 (c). The traditional RFOC is responsible for controlling the motor speed, and it is based on (Novotny; Lipo, 1996). The control signals are summed up, normalized and compared by the voltage modulator, in which the phase-shifted pulse width modulation (PS-PWM) with third harmonic injection is considered in this paper (Hagiwara; Akagi, 2009).

A Phase-Shifted PWM (PS-PWM) with third harmonic injection is the modulation strategy employed. The PS-PWM consists of comparing the carriers with the reference voltage, generating the gate signals. The angular displacements of the lower arm carriers $\theta^i_{c,l}$ are calculated by the following equation:

$$\theta^i_{c,l} = 2\pi\left(\frac{i-1}{N}\right), \tag{3.6}$$

where $i = 1, 2, ..., N$. On the other hand, the angular displacements of the upper arm carriers are given by:

$$\theta_{c,u}^{i} = \theta_{c,l}^{i} + \beta, \tag{3.7}$$

where β indicates the angular displacement among the carrier waveforms in the upper and lower arms. The angular displacements of the carrier waveforms can be chosen in terms of the desired harmonic performance. This work employs the $(2N+1)$-level modulation, as described in (Ilves et al., 2013). The angular displacement is given by:

$$\beta = \frac{\pi}{N}, \tag{3.8}$$

if N is even, and:

$$\beta = 0, \tag{3.9}$$

if N is odd.

The modulator adds, normalizes and compares the reference signal with the carrier signals (Hagiwara; Akagi, 2009; Hagiwara; Nishimura; Akagi, 2010; Hagiwara; Hasegawa; Akagi, 2013; Sahoo; Bhattacharya, 2018), as shown in Fig. 19. The normalized reference signals per phase are given by:

$$v_u^* = \frac{v_b^*}{v_{sm}^* N_{o(u)}} + \frac{v_z^*}{v_{sm}^* N_{o(u)}} - \frac{v_s^*}{v_{sm}^* N_{o(u)}} + \frac{v_{com}^*}{v_{sm}^* N_{o(u)}} + \frac{1}{2}\frac{N}{N_{o(u,l)}}, \tag{3.10}$$

$$v_l^* = \frac{v_b^*}{v_{sm}^* N_{o(l)}} + \frac{v_z^*}{v_{sm}^* N_{o(l)}} + \frac{v_s^*}{v_{sm}^* N_{o(l)}} + \frac{v_{com}^*}{v_{sm}^* N_{o(l)}} + \frac{1}{2}\frac{N}{N_{o(u,l)}}, \tag{3.11}$$

where v_u^* and v_l^* are the upper and lower voltage reference, respectively. The v_b^* is the reference of the balancing control, v_z^* is the voltage generated by the control of the circulating current and $N_{o(u,l)} = \min(N_{o(u)}, N_{o(l)})$.

3.3 Main Circuit Parameters Design

The first step to design a MMC-based electric drive is determining the dc-link voltage. The minimum dc-link voltage can be computed by:

$$v_{dc} = \sqrt{2} V_s k_{res}, \tag{3.12}$$

where V_s is the rated rms line-to-line stator voltage and k_{res} is the percentage of reserve voltage. For typical industrial medium-voltage electrical drives, the k_{res} is usually 1.2

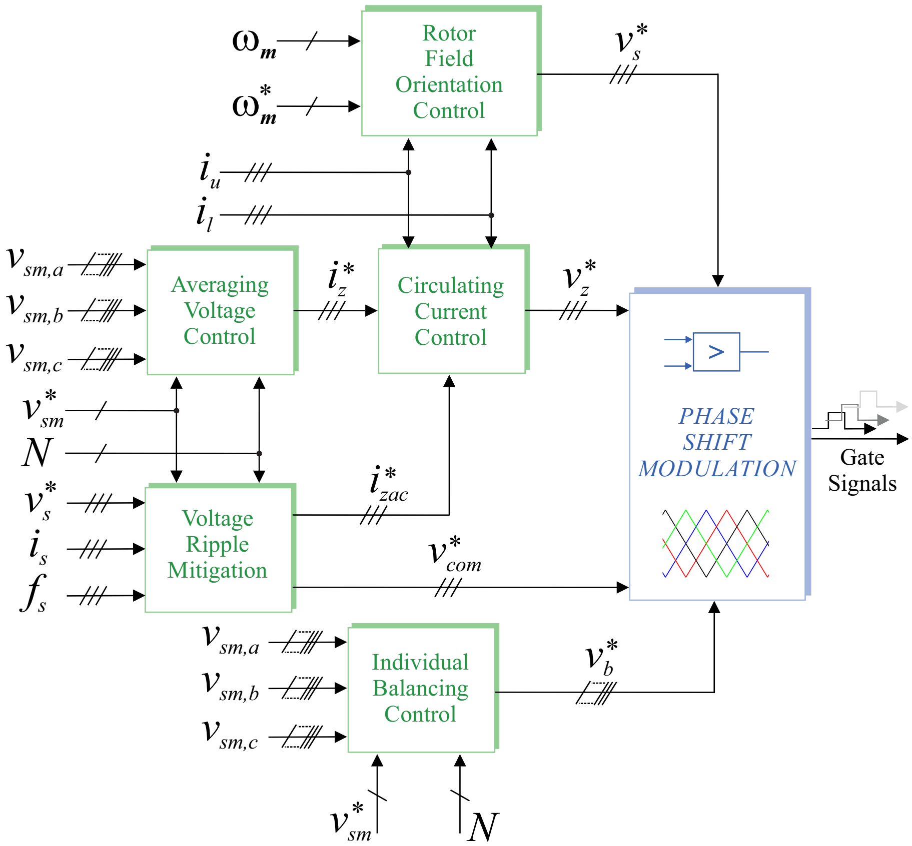

Figure 19 – Connection between the control and modulation scheme.

(ABB, 2013). The percentage of reserve voltage is used to guarantee proper operation of the MMC under transient conditions and also to compensate the voltage drop on arm and stray inductances (Marzoughi et al., 2018).

The best cost/effective design for number of SM is primarily dictated by the blocking voltage capability of the employed IGBTs. In this paper, IGBTs with blocking voltage, V_{bv}, in the range of 1.7 kV to 6.5 kV are considered. The device utilization factor, f_u can be calculated from:

$$f_u = \frac{v_{sm}^*}{V_{bv,100fit}}, \tag{3.13}$$

where $V_{bv,100fit}$ is the IGBT blocking voltage for a device failure rate of 100 failures in time (FIT) due to cosmic radiation (Islam; Guo; Zhu, 2014a). This is a typical FIT value for semiconductors used in the design of converters for HVDC systems and medium-voltage electrical drives (Islam Y. Guo, 2014; Sharifabadi et al., 2016). The reference SM voltage v_{sm}^* can be computed as:

$$v_{sm}^* = \frac{v_{dc}}{N}. \tag{3.14}$$

A higher f_u is key for an improved cost/effective design, since the semiconductor cost is a significant parameter in medium-voltage converter applications (Islam Y. Guo, 2014). Table 3 summarizes the reference SM voltage and utilization factor for some SM numbers. Considering the availability of the power semiconductors devices, the designs with 7, 11, 14, 20 and 27 have the f_u near to the unit for the classes of 6.5, 4.5, 3.3, 2.5 and 1.7 kV, respectively. Thus, such values were considered for further analysis and comparison. A low f_u means the use of unnecessarily high-cost semiconductors. In general, to use the active switching devices cost-effectively, a design must have a f_u of 0.9 or above (Islam Y. Guo, 2014).

The SM capacitance can be calculated based on the MMC energy storage requirements. According to (Ilves et al., 2014), the minimum SM capacitance is given by:

$$C = \frac{N S_n W_{conv}}{3 v_{dc}^2}, \tag{3.15}$$

where S_n is the MMC apparent power and W_{conv} is the required energy storage per MVA.

Table 3 – Utilization factor for different SM number.[a]

N	v_{sm}^* (kV)	V_{bv} (kV)	$V_{bv,100fit}$ (kV)	f_u
6	4	6.5	3.6	1.11
7	3.43	6.5	3.6	0.95
8	3	6.5	3.6	0.83
9	2.67	6.5	3.6	0.74
10	2.4	6.5	3.6	0.67
11	2.18	4.5	2.25	0.97
12	2	4.5	2.25	0.89
13	1.85	4.5	2.25	0.82
14	1.71	3.3	1.8	0.95
15	1.6	3.3	1.8	0.89
16	1.5	3.3	1.8	0.83
17	1.41	3.3	1.8	0.78
18	1.33	3.3	1.8	0.74
19	1.26	3.3	1.8	0.70
20	1.2	2.5	1.2	1.00
21	1.14	2.5	1.2	0.95
22	1.09	2.5	1.2	0.91
23	1.04	2.5	1.2	0.87
24	1	2.5	1.2	0.83
25	0.96	2.5	1.2	0.80
26	0.92	2.5	1.2	0.77
27	0.89	1.7	0.9	0.99
28	0.86	1.7	0.9	0.95

[a] Considering the rated stator voltage $V_s = 13.8$ kV and $v_{dc} = 24$ kV.

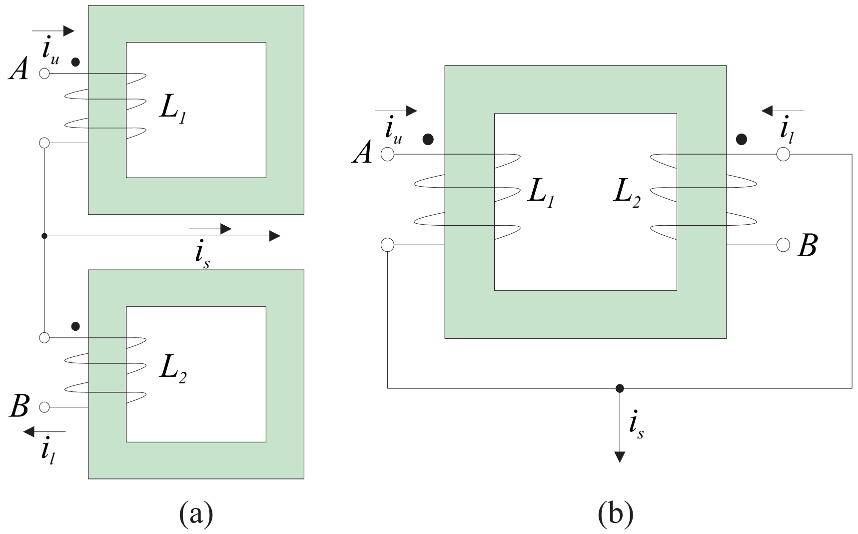

Figure 20 – Two kind of inductors configuration: (a) individual inductors; (b) coupled inductors.

A typical values of W_{conv} is approximately 60 kJ/MVA for MMC-based drive (Akagi, 2017). Typically, high-density Electronicon film capacitors are considered in each SM.

As mentioned in the previous section, this paper considers the PS-PWM. In this modulation technique, N triangular carriers are used per arm, displaced by $360°/N$, featuring an effective output frequency of (Marzoughi; Burgos; Boroyevich, 2019):

$$f_{ef} = 2N f_{sw}, \tag{3.16}$$

where f_{sw} is the carrier frequency (Marzoughi; Burgos; Boroyevich, 2019).

The arm inductance L_{arm} is used to minimize oscillations in circulating current (Harnefors et al., 2013; Farias et al., 2018). Typically, values between 0.05 to 0.15 p.u. are used for the MMC (Sharifabadi et al., 2016). In turn, when $(2N + 1)$-level PS-PWM modulation is employed, the ripple of circulating current, Δi_z, is proportional to (Li; Jones; Wang, 2017):

$$\Delta i_z \propto \frac{1}{f_{ef} L_{arm}}. \tag{3.17}$$

In order to keep similar values of circulating current ripple, f_{ef} and L_{arm} are kept constant. This means that the smaller the number of SMs, the greater the switching frequency, as discussed in (Huber; Kolar, 2017).

Fig. 20 shows two types of arm inductors physical realization. First, Fig. 20 (a) shows the use of individual inductors. In this configuration, the arm's inductances are given by:

$$L_1 = \frac{N_1^2}{\Re_1}, \tag{3.18}$$

$$L_2 = \frac{N_2^2}{\Re_2}, \tag{3.19}$$

where N_1 is the turns number of the winding 1, $\Re_1$ is the reluctance of the core 1, N_2 is the turns number of the winding 2 and $\Re_2$ is the reluctance of the core 2. In this configuration, the equivalent inductance seen from the circulating current side is a series association, given by:

$$L_{arm,z} = L_1 + L_2 = \frac{N_1^2}{\Re_1} + \frac{N_2^2}{\Re_2}. \tag{3.20}$$

In turn, the equivalent inductance seen from the motor side is a parallel association:

$$L_{arm,s} = L_1//L_2 = \frac{N_1^2 N_2^2}{N_1^2 \Re_2 + N_2^2 \Re_1}. \tag{3.21}$$

Assuming that the inductors have the same turn numbers of the winding, N_w, the material and size of the core are identical, so the same reluctance, $\Re_c$, the equivalent inductance seen from the circulating current and the motor current can be calculated by:

$$L_{arm,z} = \frac{2N_w^2}{\Re_c}, \tag{3.22}$$

$$L_{arm,s} = \frac{N_w^2}{2\Re_c}. \tag{3.23}$$

As observed, individual inductors lead to some inductance for the output current. Therefore, the arm inductors will affect the output current dynamics. This is usual for grid-connected applications. However, this will affect the current control dynamics of the machine, which is not desirable.

On the other hand, Fig. 20 (b) shows the use of coupled inductors. For this scheme, the equivalent inductance from the circulating current side can be computed by v_{AB}:

$$v_{AB,z} = L1\frac{di_z}{dt} + L2\frac{di_z}{dt} + M_{1,2}\frac{di_z}{dt} + M_{2,1}\frac{di_z}{dt}, \tag{3.24}$$

where $M_{1,2}$ is the mutual inductance between L_1 and L_2 and $M_{2,1}$ is the mutual inductance between L_2 and L_1. On the other hand, the equivalent inductance from the motor current is given by:

$$v_{AB,s} = L1\frac{di_s}{dt} + L2\frac{di_s}{dt} - M_{1,2}\frac{di_s}{dt} - M_{2,1}\frac{di_s}{dt}. \tag{3.25}$$

Making the same consideration explained above, that the inductors have the same turn numbers of the winding, the material and size of the core are identical, and considering that $M_{1,2} = M_{2,1} = M_w$, the equivalent inductance seen from the circulating current side and motor side is given by:

$$v_{AB,z} = (2L + 2M_w)\frac{di_z}{dt} = \left(\frac{2N_w^2}{\Re_c} + 2M_w\right)\frac{di_z}{dt}, \tag{3.26}$$

$$v_{AB,s} = (2L - 2M_w)\frac{di_s}{dt} = \left(\frac{2N_w^2}{\Re_c} - 2M_w\right)\frac{di_s}{dt}. \tag{3.27}$$

The mutual inductance M_w, cab be evaluated by:

$$M_w = K\sqrt{L_1 L_2}. \tag{3.28}$$

where K is the coupling coefficient. If $K = 1$ the two coils are perfectly coupled, if $K > 0.5$ the two coils are said to be tightly coupled and if $K < 0.5$ the two coils are said to be loosely coupled. Therefore, considering a good coupling, the equivalent inductance seen from the circulating current and motor side can be approximated by:

$$L_{arm,z} \approx 4L \approx \frac{4N_w^2}{\Re_c}, \tag{3.29}$$

$$L_{arm,s} \approx 0. \tag{3.30}$$

As observed, the coupled inductors lead to higher equivalent inductance for circulating current and minimal inductance for the fundamental output current, being theoretically null. Thus, the motor speed dynamics is not affected by the arm inductance (Hagiwara; Hasegawa; Akagi, 2013). Assuming the same converter, the use of coupled inductor results in lower volume and weight. Thus, coupled inductors are considered in this Thesis.

3.4 MMC Fault-Tolerant Operation

Due to several electrical, mechanical and environmental factors present in an industry, MMC is vulnerable to some types of failures or faults (Son et al., 2012). Nevertheless, the system should continue operating until maintenance can be programmed (Konstantinou; Ciobotaru; Agelidis, 2012). The MMC topology is often featured with its robustness for SM failures. Redundant SMs are inserted into each arm for fault-tolerant operation. When a fault is detected, the damaged SM should be bypassed (Son et al., 2012).

According to (Farias et al., 2018), the redundancy strategies can be classified as: Redundant operation based on Spare SMs (RSS), Redundant operation based on Additional SMs (RAS), Optimized Redundant operation based on Additional SMs (RASO) and Standard Redundant operation (SR).

The RSS strategy is a redundancy technique based on the concept of spare SMs (Son et al., 2012). During normal operations, the backup SM are bypassed. When a fault is detected, this faulty SM is replaced by the backup SM (Li et al., 2015). This technique has the advantage of operating with the number of SM constant and no control adaptation is employed. However, this technique affects the transient of all control variables, because the SMs inserted in the system are maintained discharged by the bleeder resistors (Farias et al., 2018). Since the redundant SM are not operating, this scheme is referred as cold redundancy or standby redundancy scheme.

The RAS strategy consists in operating the MMC with more SMs than the nominal number. When a fault occurs, the faulty SM is bypassed and the operating voltage of the SMs is maintained at the rated voltage (Saad et al., 2015; Choi; Han; Kim, 2016). Therefore, when a SM fails, the SMs voltages do not increase. Thus, small transients are observed on SM voltages.

On the other hand, RASO strategy operates the SMs with a reduced voltage under normal conditions, thus reducing the voltage stresses in the SM power devices and reduce power losses. When a fault is detected, the SMs voltages are increased to avoid overmodulation (Farias et al., 2018). Since the redundant SM are always operating, RAS and RASO are usually referred as hot-reserve or active redundancy strategies.

Finally, the SR strategy operating principle is similar to RASO. In this technique, when a failure occurs, the operating voltage of the SMs is increased (Konstantinou; Ciobotaru; Agelidis, 2012; Ahmed et al., 2015). This is an interesting solution for applications with high numbers of SMs, without the need to use additional SMs. The f_{us}, ratio between the v^*_{sm} and V_{bv} can be computed by:

$$f_{us} = \frac{v^*_{sm}}{V_{bv}}. \tag{3.31}$$

However, to maintain a safe operation, f_{us} can not exceed 0.6 (Farias et al., 2018). Therefore, this strategy is limited by the maximum voltage stresses at the semiconductor devices and capacitors. According (Farias et al., 2018), for the SR strategy, the redundancy factor f_r is computed by:

$$f_r = 1 - \frac{f_{us,0}}{f_{us,f}}, \tag{3.32}$$

where $f_{us,0}$ is the utilization factor under normal conditions, and $f_{us,f}$ is the utilization factor when all admissible failures occur. In many works of literature, f_r around 10% is employed (Konstantinou; Ciobotaru; Agelidis, 2012). Manipulation (3.32) and definition of the constant k_u results in:

$$k_u = \frac{f_{us,f}}{f_{us,o}} = \frac{N}{N - \text{ceil}(N f_r)}, \tag{3.33}$$

where k_u indicates the perceptual variation in the utilization factor. Since $f_{us,o} = 0.5$ is widely used, $k_u = 0.6/0.5 = 1.2$ would be the limit. However, once the SMs voltages present ripple, a safety margin is adopted. Thus, $k_u = 1.15$ is employed. Fig. 21 shows the effect of the number of SMs in the k_u ratio for $f_r = 0.1$. As observed, applications with lower number of SMs exceed the range of $k_u = 1.15$. Once MMC based drive systems typically employ few SMs, the SR strategy is not suitable because it results in large voltage stress in the SMs.

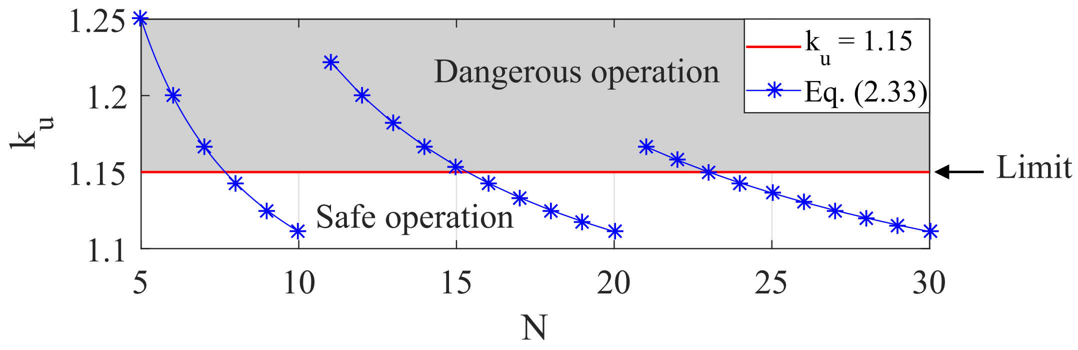

Figure 21 – Redundancy limit for SR for some number of SMs.

Regarding the implementation, the reference values for the average voltage control v^*_{avg} and the balancing control v^*_{sm}, depend on the redundancy strategy used. For the RSS and RAS strategies, the voltage reference for the individual control is calculated by:

$$v^*_{sm} = \frac{v^*_{dc}}{N}. \tag{3.34}$$

Even during faults, the average voltage references do not change in RSS and RAS strategies. Therefore, the average reference voltage per phase is calculated by:

$$v^*_{avg} = \frac{v^*_{dc}}{N}. \tag{3.35}$$

However, in the RASO strategy, when a fault is detected, the reference SMs voltages is increased. Thus, the reference voltage for all SMs and the average reference voltage for RASO strategies are computed by:

$$v^*_{sm} = \frac{v^*_{dc}}{N_{o,u,l}}, \tag{3.36}$$

$$v_{avg}^* = \frac{v_{dc}^*}{N_{o,u,l}}. \tag{3.37}$$

Table 4 shows the main characteristics of each redundancy strategy described in this chapter, where F is the number of failures in a given arm.

Table 4 – Main characteristics of redundancy strategies.

Strategy	v_{sm}^*	N_o	M	Reference
RAS	$\frac{v_{dc}}{N}$	$N+M-F$	$M = ceil(Nf_r)$	(Saad et al., 2015)
RASO	$\frac{v_{dc}}{N_o}$	$N+M-F$	$M = ceil(Nf_r)$	(Ahmed et al., 2015)
RSS	$\frac{v_{dc}}{N}$	N	$M = ceil(Nf_r)$	(Son et al., 2012; Li et al., 2015)
SR	$\frac{v_{dc}}{N_o}$	$N-F$	$M = 0$	(Liu et al., 2015)

3.5 Reliability

The reliability function, $R(t)$, and the failure rate, $\lambda(t)$ are very important factors for modeling the reliability of electronic converters. $R(t)$ represents a group of samples that can function properly for a specific time and $\lambda(t)$ is the failure rate of a system. Device failures can be caused randomly or by wear-out during operation. Wear-out failures can be reduced if proper converter design is performed, as described in (Wang; Ma; Blaabjerg, 2012). Thus, this work considered the MMC reliability modeling based on random failures (Farias et al., 2019). The reliability block diagram is shown in Fig. 22. The SM reliability function is given by (Tu; Yang; Wang, 2018):

$$R_{sm}(t) = e^{-\lambda_{sm} t}, \tag{3.38}$$

where λ_{sm} is the SM failure rate. In this work, the failure rates of the IGBTs, the capacitor and the SM control system are considered. The failure rates of the SM control system includes the IGBT drive circuits, communication system and SMs controller (Guo et al., 2018). Assuming the failure rate of each component is independent, thus:

$$\lambda_{sm} = 2\lambda_{IGBT} + \lambda_{capacitor} + \lambda_{control}. \tag{3.39}$$

The MMC consists of six arms, with N SMs in each arm. Considering that the SMs are identical and independent, the arm's reliability function can be calculated as follows (Tu; Yang; Wang, 2018):

$$R_{arm}(t) = \prod_{l=1}^{N} R_{sm(l)}(t). \tag{3.40}$$

The reliability of the MMC, of the six arms, are given by:

$$R_{MMC}(t) = \prod_{arm=1}^{6} R_{arm}(t). \tag{3.41}$$

However, Eq. (3.40) is only suitable when redundant SMs are not used. Redundant cells are operated in active or standby mode. Active mode operates with or without load sharing (Chen; Yu; Li, 2019). In this work, only the active redundancy that operates without load sharing will be considered. In this way, when a component fails, the load on the remaining functional components is not changed. Therefore, the MMC arm level reliability considering active redundancy can be assessed using the *k-out-of-n* model, provided by (Chen; Yu; Li, 2019):

$$R_{active}(t) = \sum_{p=K}^{N} C_N^p R_{sm}(t)^p (1 - R_{sm}(t))^{N-p}. \tag{3.42}$$

In turn, considering the redundancy in the standby mode, the redundant SMs are inserted in the MMC only when there is a failure in any operant SM. The reliability can be modeled as a homogeneous Poisson process with a constant rate λ_{sm} (Chen; Yu; Li, 2019). The MMC arm level reliability is given by (Tu; Yang; Wang, 2018):

$$R_{standby}(t) = \sum_{K=0}^{N-K} \frac{(\lambda_{sm} t)^K}{K!} e^{-\lambda_{sm} t}. \tag{3.43}$$

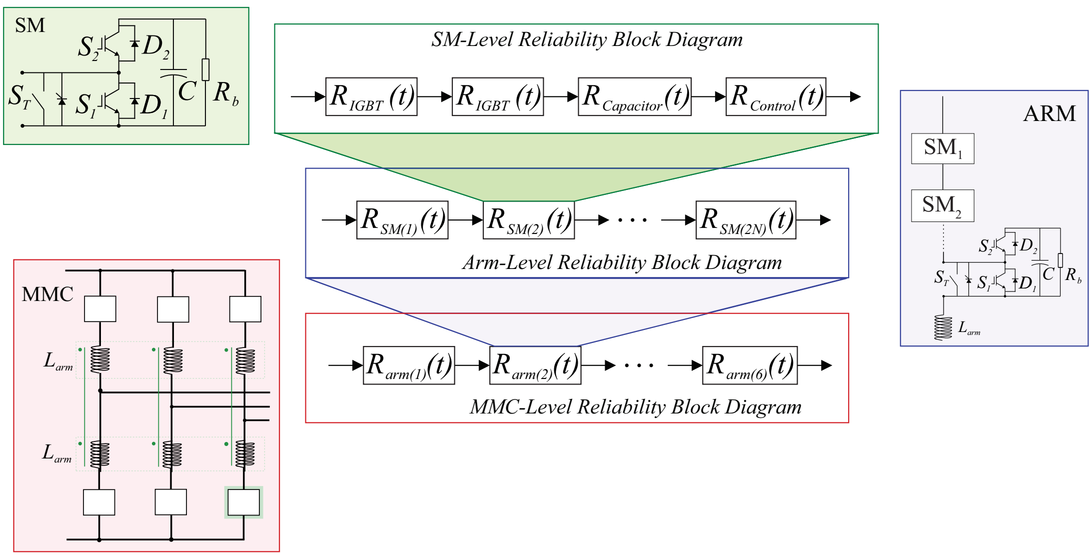

Figure 22 – Reliability block diagram of the MMC-based electric drives.

Finally, the reliability of the MMC, of the six arms, considering the active and standby redundancy techniques, are given by:

$$R_{MMC,active}(t) = \prod_{arm=1}^{6} R_{active}(t). \tag{3.44}$$

$$R_{MMC,standby}(t) = \prod_{arm=1}^{6} R_{standby}(t). \tag{3.45}$$

The number of redundant SMs, M, is calculated using an iterative method proposed in (Farias et al., 2019), whose objective is to guarantee the reliability requirement. For medium-voltage electric drives, an estimated 7-year service life is generally assumed (Wang et al., 2014; Falck et al., 2018). Therefore, the number of redundant SMs is calculated so that the converter has 99% reliability in 7 years of operation. It is worth mentioning that redundancy affects the choice of the design with the best cost-benefit, since redundancy affects the number of SM in the converter. Thus, the reliability criterion is used so that the designs with IGBTs of different blocking voltage present the same level of reliability.

3.6 Chapter Conclusions

In this chapter the topology of MMC-based electric drive were presented. In addition, the control schemes and the CMI employed were discussed. Furthermore, the design of the main components and variables were presented. Finally, some redundancy strategies and the reliability study were also presented in this chapter.

The next chapter presents and details the figures of merit used to compare and choose the MMC-based electric drive design with the best cost/benefit ratio for an industrial application.

4 Case Study and Figures of Merit

The case study employed in this work is presented in this chapter. Next, the motor parameters, power converter and mission profile are shown. Furthermore, the figures of merit used to compare and choose the MMC-based electric drive are presented. Finally, the normalized total index is presented for comparison of the different designs of MMC-based drives to chosen the best cost/effective ratio for a given industrial application.

4.1 Case Study

The case study used in the tests carried out in this work consists of a MMC-based drive with 16 MW - 13.8 kV induction motor which drives an industrial blower. The motor parameters are reported in Table 5. The parameters of the motor equivalent circuit were estimated from these plate data, according to the algorithm proposed by (Pedra; Corcoles, 2004).

Table 5 – Induction motor parameters.

Parameter	**Value**
Rated active power (P_r)	16 MW
Rated rms line-to-line stator voltage ($V_{s,r}$)	13.8 kV
Rated stator current ($I_{s,r}$)	801 A
Rated frequency ($f_{s,r}$)	60 Hz
Rated rotational speed (n_m, r)	1795 rpm
Rated power factor	0.9
Rated efficiency (η)	97.4%
Number of poles (P)	4
T_{max}/T_{rated} ratio	2.4

The variations from the values of the plate data when they are calculated from the parameters of the equivalent circuit found by the algorithm are shows in Table 6. As noted, the algorithm was able to estimate the parameters of the plate data with a maximum error smaller than 2.5%. In turn, the estimated equivalent circuit parameters can be analyzed in Table 7.

For this study, an MMC with a power of 20 MVA, a voltage of 13.8 kV and a nominal current of approximately 840 A was considered. Table 8 shows the part numbers employed in the MMC designs. Five different HiPak IGBTs modules with blocking voltage capability range between 1.7 kV and 6.5 kV are considered. Commercially available modules with rated current close to 800 A are selected.

Table 6 – Percentage errors obtained for the values shown on the motor plate data.

Parameter	Percentage errors (%)
Rated active power	0.014268
Rated stator current	1.1274x10^{-6}
Rated power factor	2.3989
Rated efficiency	2.3093
T_{max}/T_{rated} ratio	8.5763x10^{-5}

Table 7 – Parameters obtained by the implemented algorithm.

Parameter	Estimated value
Rotor resistance (R_r)	0.02923 Ω
Stator resistance (R_s)	0.027552 Ω
Magnetization inductance (L_m)	87.9 mH
Stator leakage inductance (L_{ls})	3.1 mH
Rotor leakage inductance (L_{lr})	3.1 mH

Table 8 – HiPak IGBT modules specifications for proposed designs.

Voltage (V)	Current (A)	Part Number	Manufactures
1700	800	5SND 0800M170100	ABB
2500	800	CM800HB-50H	Mitsubishi
3300	800	5SNA 0800N330100	ABB
4500	800	5SNA 0800J450300	ABB
6500	750	5SNA 0800J450300	ABB

The industrial mission profile used, characterized by the motor speed and ambient temperature where the converter is located, are obtained from measurements of a steel industry in southeastern Brazil, and are shown in Fig. 23. The conjugate profile is approximate, assuming a quadratic load characteristic.

Finally, the MMC specifications for each project are shown in Table 9. Most of these parameters were computed based on the equations of Chapter 3. The failure rates considered for the reliability study are based on statistical data, as described in (Guo et al., 2018). The simulations are performed in PLECS/MATLAB aiming to validate the proposed methodology and perform the comparison.

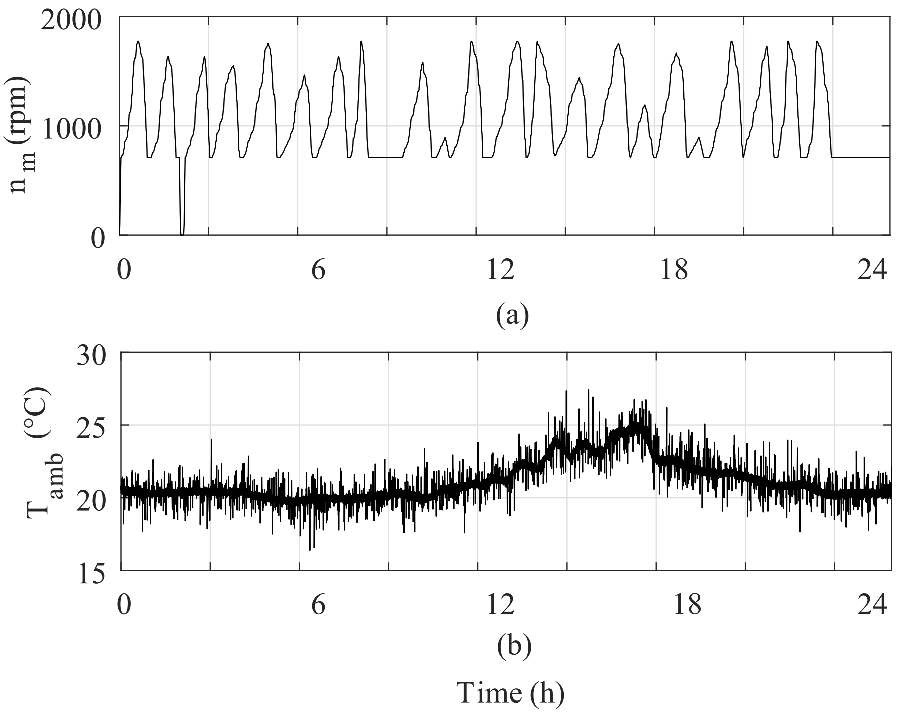

Figure 23 – Industrial mission profile: (a) Motor speed; (b) Ambient temperature.

Table 9 – MMC ratings for selected designs.

	MMC Design				
Parameter	**I**	**II**	**III**	**IV**	**V**
N	7	11	14	20	27
Levels	15	23	29	41	55
v_{dc} (kV)	24	24	24	24	24
v_{bv} (kV)	6.5	4.5	3.3	2.5	1.7
v_{sm}^* (kV)	3.43	2.18	1.71	1.20	0.89
S_n (MVA)	20	20	20	20	20
C (mF)	5	7.86	10	14.28	19.28
L_{arm} (mH)	7.7	7.7	7.7	7.7	7.7
R_{arm} Ω	0.14	0.14	0.14	0.14	0.14
f_{sw} (Hz)	945	602	473	348	245
f_{ef} (kHz)	13.23	13.23	13.23	13.23	13.23
R_{heat} (K/kW)	1	7	25	45	70
λ_{IGBT} (failures/year)	0.0014	0.0012	0.0013	0.0012	0.0013
$\lambda_{capacitor}$ (failures/year)	0.0018	0.0018	0.0018	0.0018	0.0018
$\lambda_{control}$ (failures/year)	0.0032	0.0032	0.0032	0.0032	0.0032

4.2 Figures of Merit

4.2.1 Efficiency

The efficiency is an significant criteria when selecting a best cost-effect converter for electrical drives. As mentioned before, motor systems currently account for 30% of global electricity demand (IEA, 2019). In this work, the metric used as a figure of merit for comparison is derived from the loss of energy over a daily cycle. Conduction and switching losses were estimated with look-up tables, as described in (Farias, 2019) and illustrated in Fig. 24. The data needed to estimate conduction losses, switching losses and thermal impedances of the devices are obtained from the manufacturer datasheets.

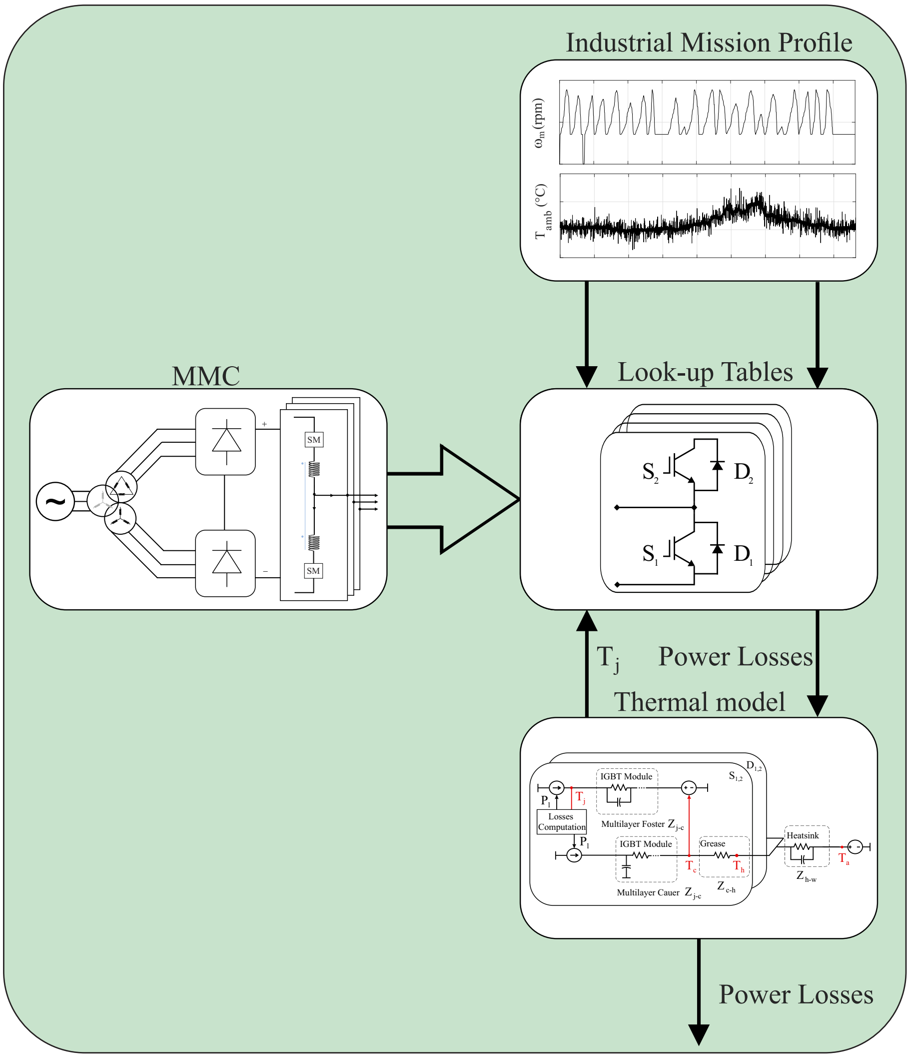

Figure 24 – Power losses estimation of the MMC.

4.2.2 Volume

For the volume metric, the converter volume is estimated by the sum of the individual volumes of the following components: IGBTs, capacitors, inductors, heatsinks and ventilation system. The volume of the IGBTs, V_{IGBT}, can be calculated using the dimensions (width, height and length) informed in the manufacturers data sheets.

In turn, the capacitor volume is estimated following the methodology proposed in (Huber; Kolar, 2017), in which the energy storage requirement is used as a premise. For the MMC, the stored energy, E_C, is calculated by (Farias et al., 2018):

$$E_C = \frac{3Cv_{dc}^2}{N}. \tag{4.1}$$

Thus, assuming a volume constant per stored energy, k_E, of 6.3 cm^3 /J (Huber; Kolar, 2017) the volume of the capacitors, V_{cap}, can be obtained as:

$$V_{cap} = E_C K_E. \tag{4.2}$$

The volume of the inductors is estimated from values presented in (Marzoughi; Burgos; Boroyevich, 2019), where a case study of a MMC-based electric drive of 5 MVA, 13.8 kV and 2 mH arm inductance is developed. The total volume of the 6 arm inductors of this converter was 0.02773 m^3. With these values in place, a linear scale was performed for the case study used in the present work, a MMC-based electric drive of 20 MVA, 13.8 kV and 7.7 mH of arm inductance. In this way, the volume of this component is calculated assuming that each inductor is made by the association of 4 inductors in parallel (in order to guarantee the same current circulation capacity) and an association of 15 of these sets of inductors in series (to obtain the same inductance).

For heatsinks and ventilation systems, the volume is obtained through (Huber; Kolar, 2017):

$$V_{heat} = \frac{1}{CSPI \times R_{heat}}, \tag{4.3}$$

where $CSPI$ is the cooling system performance index, and R_{heat} is the thermal resistance of the heatsink to the ambient. For cooling systems using forced ventilation, typical values of 10 W / (Kdm ^{3}) are used (Huber; Kolar, 2017). The thermal resistance of the heatsink to the ambient is calculated to maintain the same junction temperature, T_j, of the most stressed device of all designs, within a safe limit (junction and case temperatures below 115 °C and 100 °C, respectively). Finally, a volume compensation factor $C_v = 0.7$ is considered in order to consider the component spacing in the converter, due to the different geometric characteristics and insulation of each component (Kolar et al., 2010).

4.2.3 Silicon Area

The switched power is an indirect estimate of the converter's silicon area, which in turn directly affects the converter investment cost. The switched power, P_{sw}, is calculated by (Siddique et al., 2016):

$$P_{sw} = N_{semi} V_{bv} I_c, \tag{4.4}$$

where N_{semi} is the number of semiconductor devices used and I_c is the rated collector current of the device.

4.2.4 Complexity

Complexity is also a very important figure of merit for making the most cost-effective choice of project. Complexity is often assessed in terms of the number of arithmetic and logical operations (ALO) performed in the converter modulation system (Islam; Guo; Zhu, 2014b). However, in this work, the complexity is assessed indirectly through the number of sensors (current and voltage) necessary to carry out the control and operation of the MMC.

Therefore, the complexity can be calculated as:

$$Complexity = 6N + 6. \tag{4.5}$$

As observed, the increase in the number of SMs in the converter implies a linear increase in complexity.

4.3 Total Index

In order to compare the different MMC designs based on different metrics, a normalized index, k_x, is calculated by:

$$k_x = \frac{x - x_{min}}{x_{max} - x_{min}}, \tag{4.6}$$

where x is the metric evaluated (efficiency, volume, silicon area and complexity), x_{min} and x_{max} are the minimum and maximum values for this indicator, respectively. To compare the different designs, the total normalized index is calculated by:

$$k_t = k_{effic.} + k_{vol.} + k_{sil.a.} + k_{compl.}. \tag{4.7}$$

It is important to note that the present work assumes that all normalized indexes have the same impact factor. However, according to the needs of the design, different weights can be assigned to the metric in which it is desired to have greater or lower relevance (Júnior et al., 2019).

4.4 Chapter Conclusions

In this chapter the case study employed in this work are presented. The details of the motor, power converter and mission profile are illustrated. Furthermore, the figures of merit used to compare and choose the MMC-based electric drive project with the best cost/benefit ratio for an industrial application are presented. The figures of merit used in this work are: efficiency, volume, silicon area and complexity. Finally, the way of comparison the different designs of MMC-based drives to chosen the best cost/benefit ratio for an industrial application are illustrated.

The next chapter presents the results obtained in this work. Initially, the results of the dynamics of the MMC-based electric drives are also shown and discussed in the next chapter. In sequence, a comparison will be made in order to choose the design with the best cost-benefit based on efficiency, volume, silicon area and complexity.

5 Results

In this chapter, the results were presented. For didactic reasons, since the dynamic performance is similar for all designs (I to V), the dynamics simulation results presented are only for the design III. The simulations are performed in PLECS/MATLAB software. This chapter shows the dynamic performance of the MMC-based drive (mechanical and electrical). Furthermore, it was observed that the use of redundancy, active or standby, makes it considerably increase the reliability of the system. Finally, the best cost-benefit ratio for redundancy in active and standby mode are compared.

5.1 Dynamic Performance

Fig. 25 shows the speed profile and torque applied to the system. The motor speed profile adopted in this paper can be observed in Fig. 25 (a). The motor is accelerated from 2 to 22 seconds, and, in steady-state, the motor speed is maintained at 1800 rpm. In addition, this figure illustrates the speed error during the start-up, which results in a maximum error of 2.1 rpm in $t = 2$ s. The small speed variation in $t = 8.6$ s is caused by the end of the CMI used. Fig. 25 (b) shows the load torque applied to the motor shaft and the electromagnetic torque developed. The load torque used is based on SDW software,

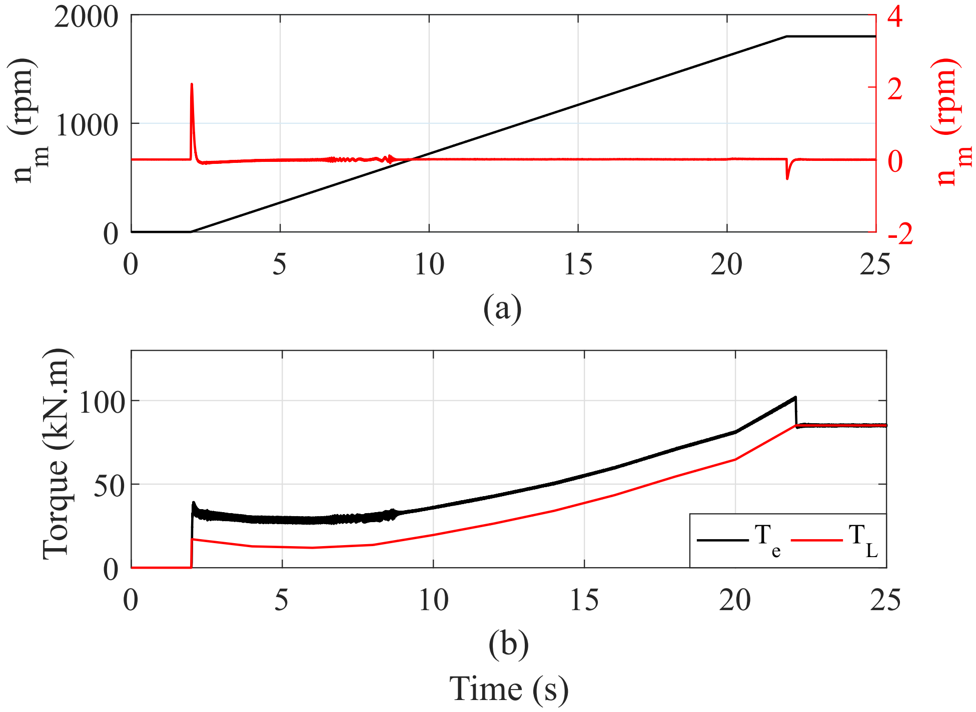

Figure 25 – Start-up of the MMC-based electric drive for design III: (a) torque; (b) mechanical speed and speed error.

developed by WEG (WEG, 2021). This torque is a quadratic function of the motor speed, usually applied to high power industrial blower. The difference in the transient is due to the acceleration of the motor, and the developed torque must be higher than the load torque. The oscillations present at t = 8.6 s are due to the end of the CMI. There is a very low ripple in the torque, which tends to minimize vibrations in the motor, since the converter has 14 SMs and, consequently, 31 levels of phase voltage.

Fig. 26 shows the converter electrical dynamics. Initially, all capacitors of the SMs were considered charged. At 0.1 seconds, the direct axis current was inserted in order to magnetize the motor. This behavior can be analyzed in the stator phase currents, shown in Fig. 26 (a), when the dc component is applied in the machine. After 2 seconds, a speed ramp was applied to accelerate the motor. At this time, the CMI strategy was inserted

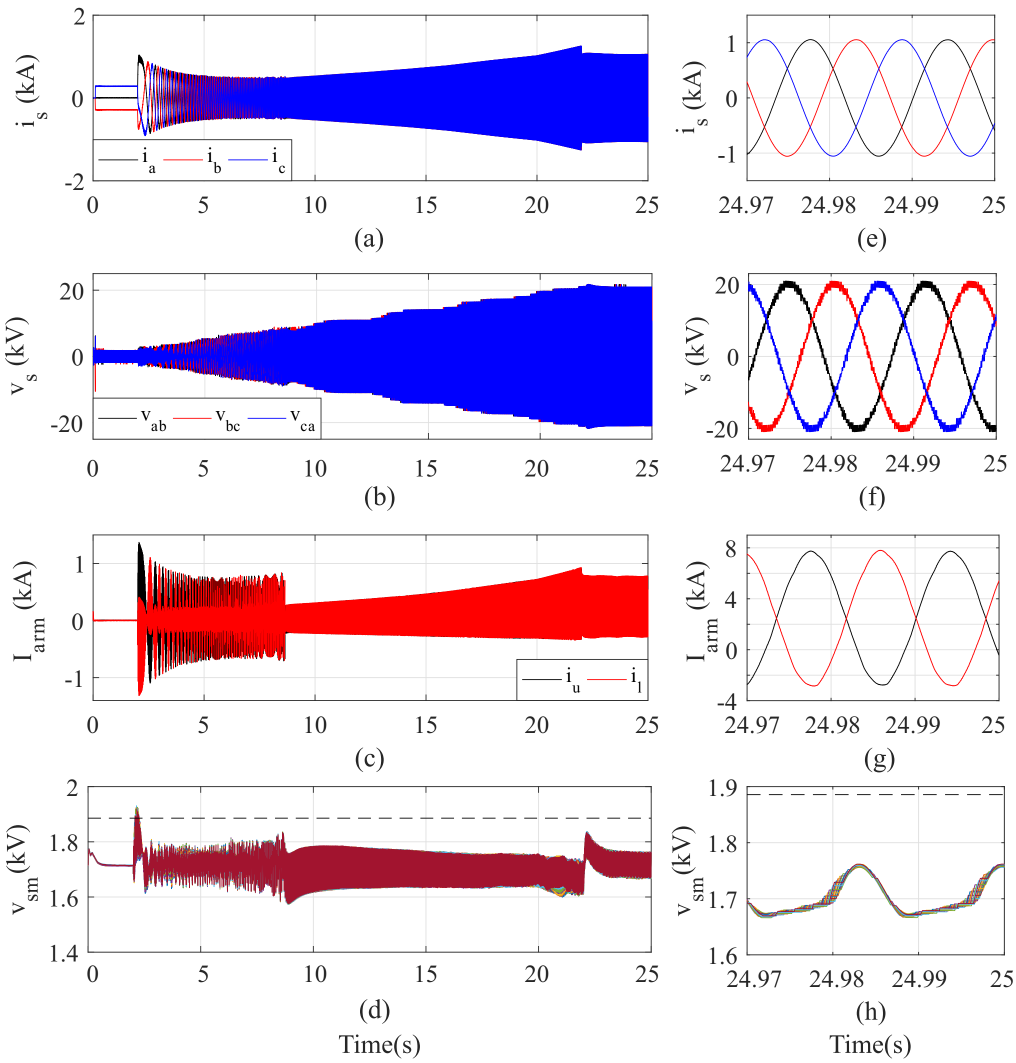

Figure 26 – Start-up of the MMC-based electric drive system for design III: (a) Stator currents; (b) Stator voltages; (c) Arm currents; (d) SM voltages of the upper arm; (e) Detail of stator currents; (f) Detail of stator voltages; (g) Detail of arm currents; (h) Detail of SM voltages of the upper arm.

to mitigate ripple under lower capacitor voltages frequency. In addition, the same figure shows a quadratic increase in the amplitude of the currents, which is also presented in Fig. 25 (b). When the motor reaches 1800 rpm, a small drop is observed in the stator currents and arm currents.

The line-to-line stator voltages are illustrated in Fig 26 (b). The oscillations observed up to $t = 8.3$ s are due the CMI, which is used to mitigate the voltage capacitor ripples at low speed. In steady-state, the stator voltage THD is 4.48%. Moreover, Fig. 26 (c) illustrates the insertion of the i^*_{zac}. This component is injected into the system until $t = 8.6$s, when the frequency applied to the motor is lower than 20 Hz. Finally, the SMs capacitor voltages of the upper arm for the a-phase are shown in Fig. 26 (d). As observed, the capacitor voltages in the steady-state have a ripple of 3.5%, that is, within the 10% dashed band in the figure. During the transient, the instantaneous value reaches a maximum of 12%.

Furthermore, considering the mission profile data, the junction temperature of the semiconductor devices in a SMs is illustrated in Fig. 27. As observed, the junction temperature variations follow closely the mission profile, Fig. 23 (a). As shown, the maximum junction temperature is 110 °C. This indicates a proper and consistent heatsink design, since the maximum temperature is kept below the limit.

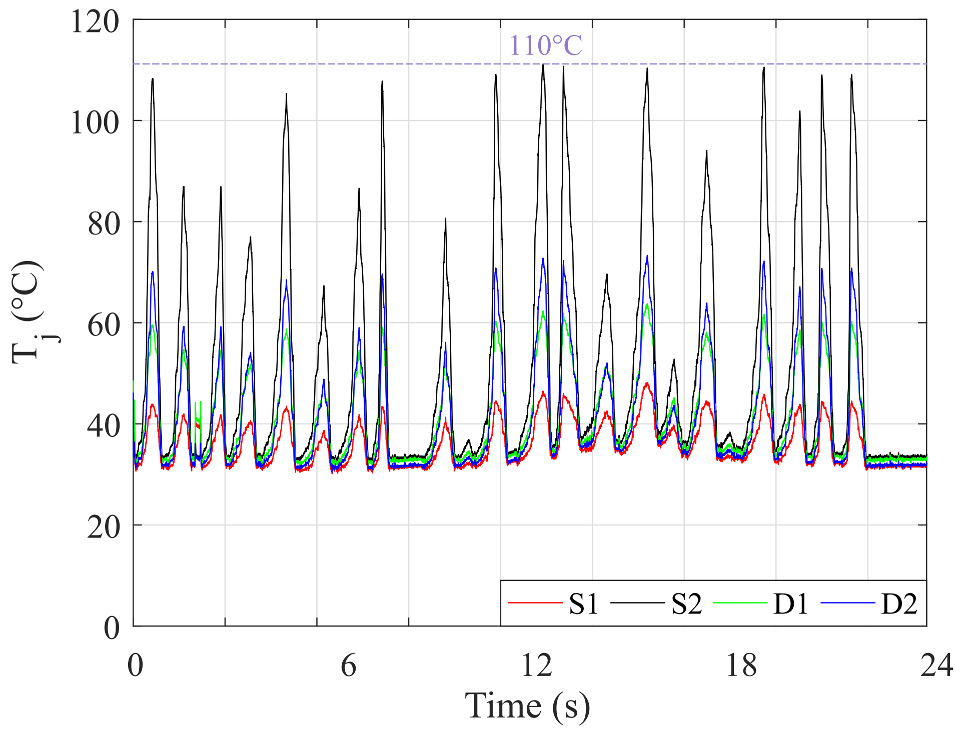

Figure 27 – Junction temperature for design III.

Finally, the semiconductors power losses of the MMC, for each speed of operation and design are shown in Fig. 28. As observed, the design that contains the IGBT with the lowest blocking voltage has the lowest power losses. At the rated speed, the design V has 22% less power losses compared with the designs III and IV, 32% less power losses compared with the design II and 46% less than to the design I. This can be related to two factors: lower conduction losses of the devices (lower voltage drop in conduction) and lower switching frequency required.

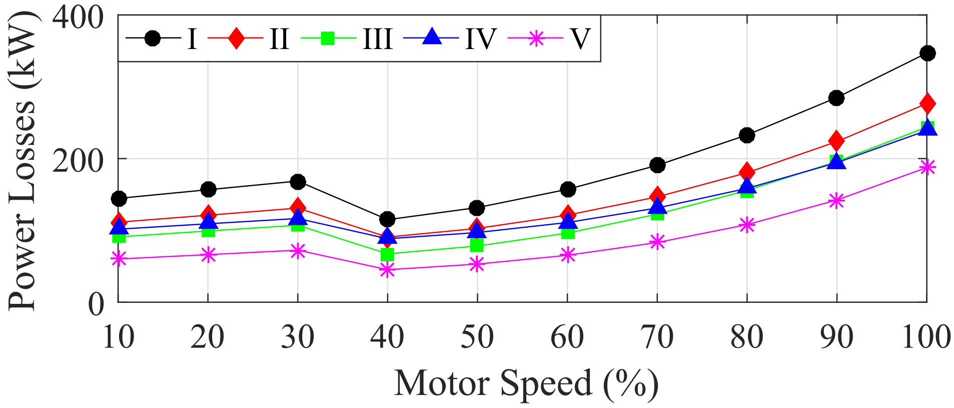

Figure 28 – Semiconductors power losses of the MMC (percentage of the nominal motor speed).

5.2 Benchmarking

The reliability of the MMC without redundancy, is shown in Fig. 29 for all designs. As expected, design I has the highest reliability, due to the smallest number of components. The reliability in 7 years of operation without redundancy is only 0.1567 for this project, and can reach up to 0.0058 for the design V, with the largest number of components.

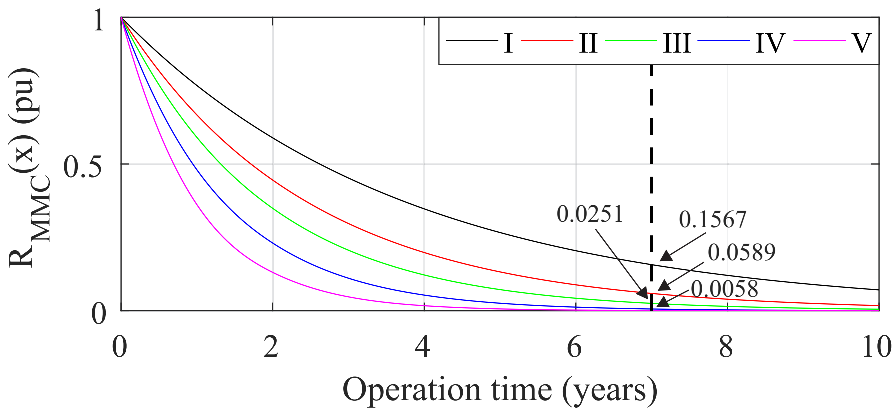

Figure 29 – MMC reliability without redundancy.

In turn, when redundancy is employed, reliability can be increased to meet design requirements. Fig. 30 illustrates the reliability of the MMC considering the active mode redundancy. In this regard, the design II achieved the highest reliability, 0.9984 in 7 years of operation. It is important to note that all projects have a reliability above 0.99 in 7 years of operation. This shows that the calculation of M was performed correctly. The differences observed between the projects are associated with rounding, since M must be an integer.

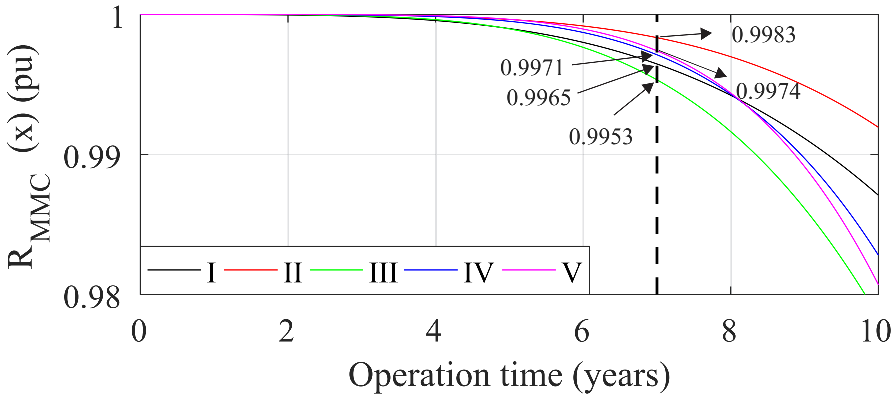

Figure 30 – MMC reliability with active mode redundancy.

In addition to redundancy in active mode, standby mode redundancy was also considered. The result for the MMC reliability in this redundancy strategy is shown in Fig. 31. In this case, design IV showed the highest reliability, 0.9984 for 7 years of operation. Differences are observed between the two types of redundancy as they require different values of M. Essentially, standby mode redundancy requires fewer redundant SMs than active mode redundancy.

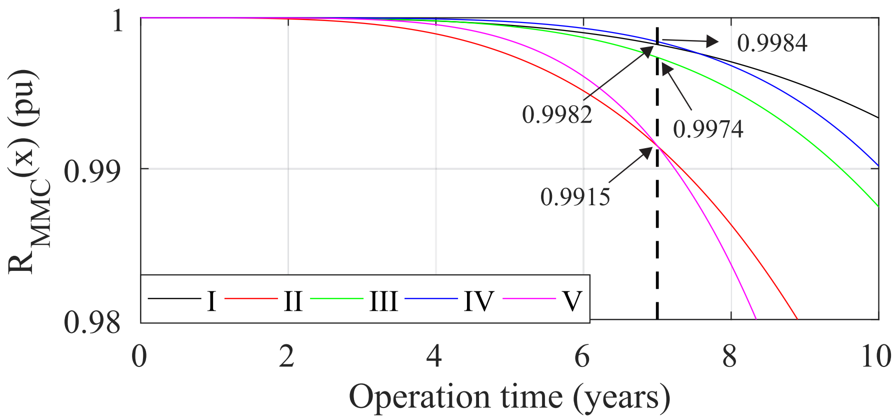

Figure 31 – MMC reliability with standby mode redundancy.

It is important to note that the fact that the reliability is very low without the use of redundancy strategies, it is not interesting to market a MMC-based electrical drive without considering some type of redundancy. It is possible to notice that as redundant SMs are inserted in the circuit, the reliability of the converter improves significantly. Thus, for a fair comparison, this work considers that the goal of reliability is a requirement of the project.

In order to choose the best design for redundancy in active mode and redundancy in standby mode, decision making is carried out using the metrics of complexity, silicon area, converter volume and efficiency. Table 10 shows the general comparison of each design taking into account redundancy in active mode.

Table 10 – General comparison of each design considering the active mode redundancy.

	MMC design				
Parameters	I	II	III	IV	V
N	7	11	14	20	27
M	3	4	4	5	6
Number of IGBTs	120	180	216	300	396
f_u	0.95	0.97	0.95	1.00	0.99
Number of sensors	66	96	114	156	204
P_{sw} (MVA)	585	648	570.2	600	538.5
Volume m^3	22.34	15.61	14.38	14.32	14.15
Daily energy losses (kWh)	4254	3634	2667	3803.8	1920

The design I presents the least complexity, a metric that is assessed indirectly through the number of sensors (arm currents and SMs voltage). Regarding the silicon area, measured indirectly through the switched power, the design V presents the best result, with the lowest switched power. In addition, the design V has the lowest volume, mainly due to the greater resistance of the heatsink. According to (4.3), high values of the thermal resistance of the heatsink to the environment favor the reduction of the volume. Finally, the design V also presents the best efficiency, following the trend shown in Fig. 24.

From the total normalized index and the results presented in Table 10, the comparison graph for the individual and total index is shown in Fig. 32 (a) and (b), respectively. To choose the design with the best cost-benefit ratio, one must find the one with the lowest overall k_t index. Therefore, for redundancy in active mode, the design III, which is based on IGBTs with a blocking voltage of 3.3 kV, is selected. It is observed that this project presents a moderate performance in all the metrics evaluated.

In turn, Table 11 shows the general comparison of each project taking into account the redundancy in the standby mode. The result was similar to that of redundancy in active mode. Project I has the least complexity. In turn, Project V has the smallest area of silicon, the lowest volume and the highest efficiency.

Applying the data from Table 11 in (4.7), the comparison graph for the individual and total index for standby mode redundancy is obtained, as illustrated in Fig. 33 (a) and (b). In this case, the design V, based on IGBTs with a 1.7 kV blocking voltage, has the lowest k_t index. It is interesting to note that the low silicon area, low volume and high efficiency made up for the complexity of this design.

Furthermore, Fig. 34 shows the comparison between project III (best cost-benefit ratio for redundancy in active mode) and project V (best cost-benefit ratio for redundancy

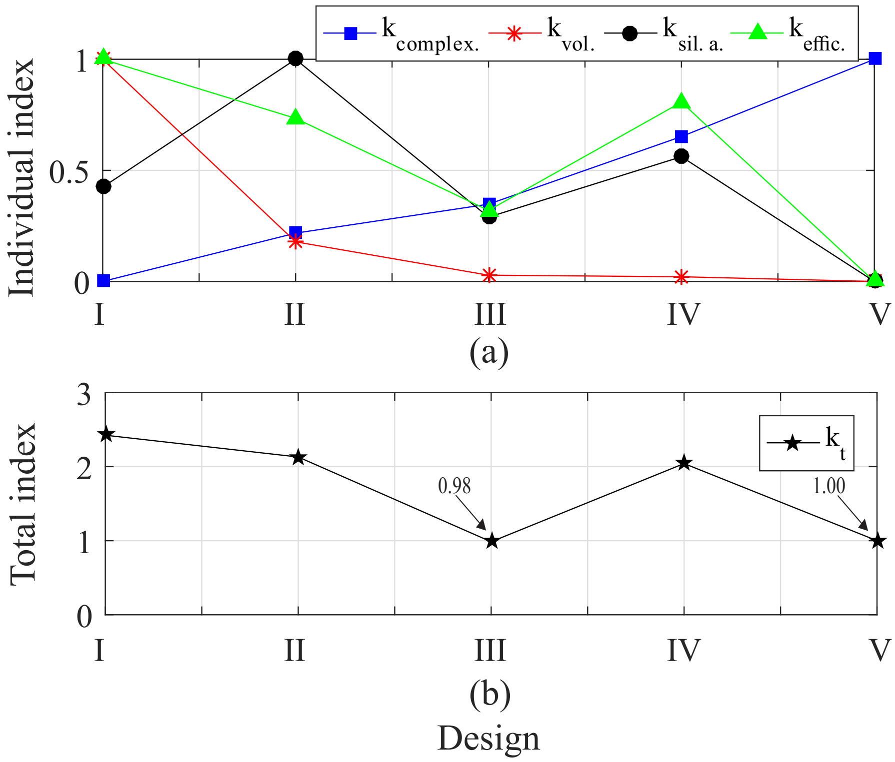

Figure 32 – Active mode redundancy: (a) individual index; (b) total index.

Table 11 – General comparison of each design considering the standby mode redundancy.

Parameters	MMC design I	II	III	IV	V
N	7	11	14	20	27
M	3	3	4	5	5
Number of IGBTs	120	168	216	300	384
f_u	0.95	0.97	0.95	1.00	0.99
Number of sensors	66	90	114	156	198
P_{sw} (MVA)	585	604.8	570.2	600	522.2
Volume m^3	22.34	15.47	14.38	14.32	14.13
Daily energy losses (kWh)	2978	2665	2074	3043	1571

in standby mode). Standby mode redundancy has an advantage in the area of silicon, volume and efficiency, but loses in complexity, due to the greater number of sensors.

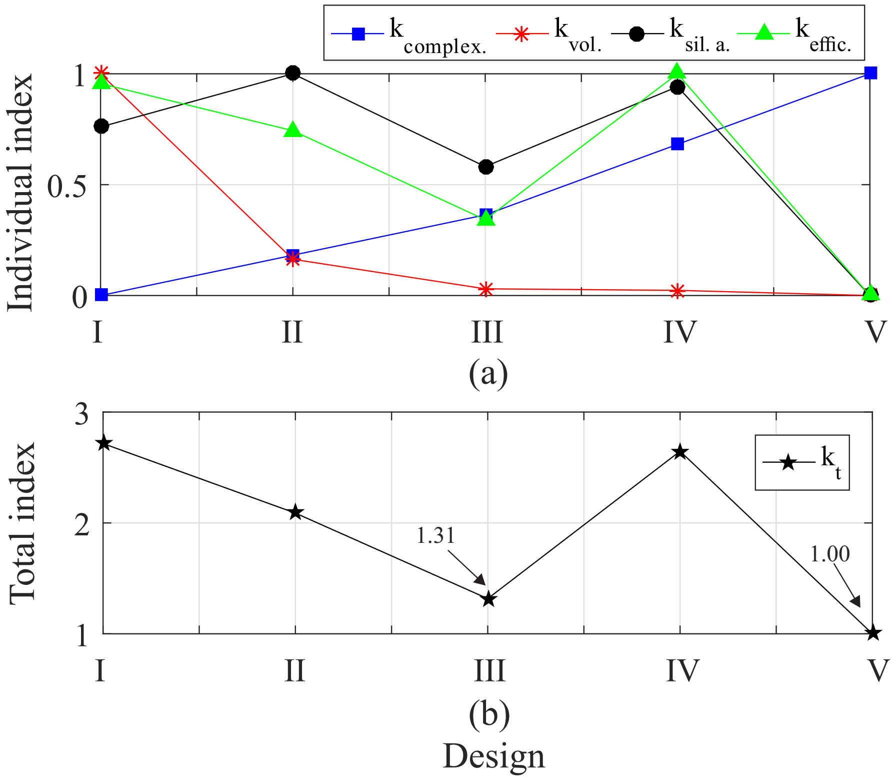

Figure 33 – Standby mode redundancy: (a) individual index; (b) total index.

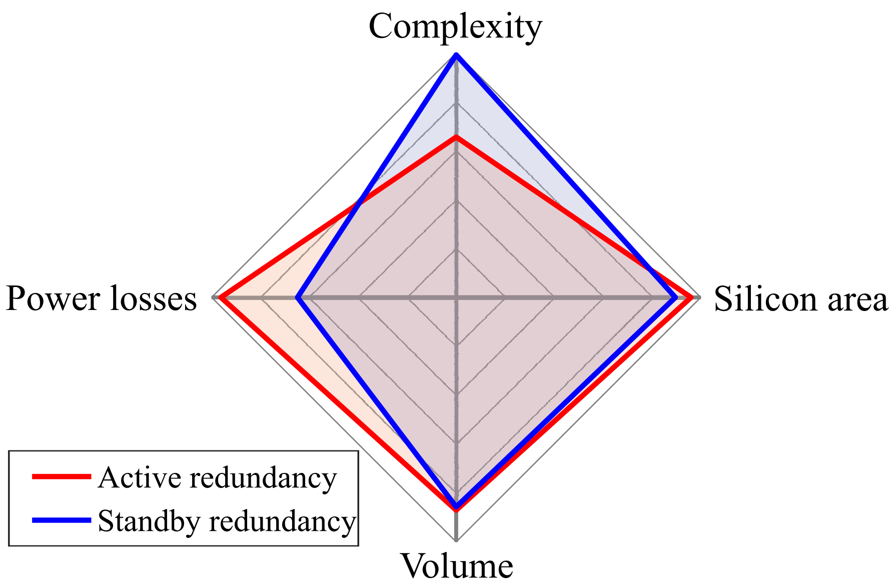

Figure 34 – Comparison between the best redundancy design in active mode (design III) with the best in standby mode (design V).

5.3 Chapter Conclusions

In this chapter, the results were presented. As observed, this chapter shows the dynamic performance of the MMC-based drive (mechanical and electrical). Furthermore, it was observed that the use of redundancy, active or standby, makes it considerably increase the reliability of the system. In this case, the design III presented the best advantage for active redundancy and design V presented the best result for standby redundancy.

The next chapter draws the conclusions of this Thesis. In addition, continuity proposals have also been proposed.

6 Closure

6.1 Conclusions

This thesis proposed a methodology to select the optimal blocking voltage for a MMC-based electric drive system, taking into account the same reliability requirements of the application. IGBTs with blocking voltage in the range of 1.7 to 6.5 kV were used in the comparison. The comparison is made based on the metrics of converter efficiency, volume, silicon area and complexity.

A case study of an industrial blower powered by a 13.8 kV - 16 MW induction motor was considered. The mission profile data is obtained from a steel industry in southeastern Brazil. The results show that the optimal class of IGBTs depends on the type of redundancy analyzed. Regarding redundancy in active mode, the 3.3 kV voltage class was the most advantageous, considering that the designs have a reliability above 99 % in 7 years of operation. This project has a moderate complexity, efficiency and silicon area and low volume. Thus, it presented the lowest total index, k_t, qualifying this project as the best in terms of cost-effective. In turn, considering the redundancy in the standby mode and the same reliability requirements for the designs, the voltage class of 1.7 kV was superior to the others. Despite the high complexity, this project has high efficiency, low silicon area and volume, presenting the lowest k_t than the other designs.

It is worth mentioning that, according to the reliability requirement, the project with the best cost-effective ratio can change, since the number of redundant SMs needed will be changed. This will affect the metrics used (complexity, volume, silicon area and efficiency). It is important to note that the methodology used in this work can be extended to other applications and methodologies for estimating reliability, volume and complexity.

6.2 Future Works

Although many aspects were studied and documented in the present Master Thesis, there are still a lot of improvements which can be implemented. From the author point of view, the following topics can be approached in further works:

- analysis of electrical drives for different voltage and power ranges;
- include physical design of inductors to make the volume estimate more trustworthy;
- carry out the designs considering a range of switching frequencies and compare the best designs of each technology in terms of power density;

- experimental implementation in a small scale prototype.

References

ABB. *Voltage ratings of high power semiconductors.* : Application note 5SYA 2051, 2013. 52

ABB. *MEGADRIVE-LCI.* : 3BHT490112R0001, 2018. REV E. 36

ABB. *Active Front End Drive Technologies.* : LVD-PNTN19U-EN, 2019. REV A. 35

Abbondanti, A. *Load Commutated Inverter (LCI) Induction Motor Drive.* : U.S. Patent, 1989. 4 870 338A. 36

Abu-Rub, H.; Bayhan, S.; Moinoddin, S.; Malinowski, M.; Guzinski, J. Medium-voltage drives: Challenges and existing technology. *IEEE Power Electronics Magazine*, v. 3, n. 2, p. 29–41, 2016. 27, 28, 29, 30, 41

Abu-Rub, H.; Holtz, J.; Rodriguez, J.; Baoming, G. Medium-voltage multilevel converters—state of the art, challenges, and requirements in industrial applications. *IEEE Transactions on Industrial Electronics*, v. 57, n. 8, p. 2581–2596, 2010. 29, 40, 41

Abu-Rub, H.; Iqbal, A.; Guzinski, J. *High Performance Control of AC Drives with MATLAB/Simulink Models.* : John Wiley and Sons, Ltd, 2012. 1-17 p. ISBN 9781119969242. 28

Abu-Rub, H.; Malinowski, M.; Al-Haddad, K. *Power Electronics for Renewable Energy Systems, Transportation and Industrial Applications.* : John Wiley and Sons, Ltd, 2014. ISBN 9781118755525. 28

Ahmed, N.; Ängquist, L.; Antonopoulos, A.; Harnefors, L.; Norrga, S.; Nee, H. P. Performance of the modular multilevel converter with redundant submodules. In: *IECON 2015 - 41st Annual Conference of the IEEE Industrial Electronics Society*. 2015. p. 003922–003927. 57, 59

Akagi, H. Multilevel converters: Fundamental circuits and systems. *Proc. of the IEEE*, v. 105, n. 11, p. 2048–2065, Nov 2017. ISSN 0018-9219. 30, 35, 36, 40, 41, 43, 54

Alesina, A.; Venturini, M. G. B. Analysis and design of optimum-amplitude nine-switch direct ac-ac converters. *IEEE Transactions on Power Electronics*, v. 4, n. 1, p. 101–112, 1989. 34

Andonov, Z.; Gjorgjeski, D.; Efremov, Z.; Cvetkovski, G.; Jeftenic, B.; Arsov, G. Medium voltage inverter for energy savings with kiln fan in cement industry. In: *2012 15th International Power Electronics and Motion Control Conference (EPE/PEMC)*. 2012. p. DS2a.11–1–DS2a.11–5. 27

Antonopoulos, A.; Ängquist, L.; Norrga, S.; Ilves, K.; Harnefors, L.; Nee, H. Modular multilevel converter ac motor drives with constant torque from zero to nominal speed. *IEEE Transactions on Industry Applications*, v. 50, n. 3, p. 1982–1993, May 2014. ISSN 0093-9994. 30, 42, 43, 49

Beltrame, F.; Sartori, H. C.; Pinheiro, J. R. Energetic efficiency improvement in photovoltaic energy systems through a design methodology of static converter. *Journal of Control, Automation and Electrical Systems*, v. 27, n. 1, p. 82–92, February 2016. 31

Ben-Brahim, L.; Gastli, A.; Yoshino, T.; Yokoyama, T.; Kawamura, A. Review of medium voltage high power electric drives. *IEEJ Journal of Industry Applications*, v. 8, n. 1, p. 1–11, 2019. 29

Benshaw. *M2l 3000 Series Medium Voltage Motor Drive.* 2018. Available in: <http://www.benshaw.com/uploadedFiles/Literature/Benshaw%20M2L%20Brochure.pdf>. 43

Bernet, S. Recent developments of high power converters for industry and traction applications. *IEEE Transactions on Power Electronics*, v. 15, n. 6, p. 1102–1117, 2000. 27

Bruckner, T.; Bernet, S. Loss balancing in three-level voltage source inverters applying active npc switches. In: *2001 IEEE 32nd Annual Power Electronics Specialists Conference*. 2001. v. 2, p. 1135–1140 vol.2. 40

Bruckner, T.; Bernet, S.; Guldner, H. The active npc converter and its loss-balancing control. *IEEE Transactions on Industrial Electronics*, v. 52, n. 3, p. 855–868, 2005. 39, 40

Busquets-Monge, S.; Alepuz, S.; Bordonau, J.; Peracaula, J. Voltage balancing control of diode-clamped multilevel converters with passive front-ends. *IEEE Transactions on Power Electronics*, v. 23, n. 4, p. 1751–1758, 2008. 40

Busse, D.; Erdman, J.; Kerkman, R. J.; Schlegel, D.; Skibinski, G. Bearing currents and their relationship to pwm drives. *IEEE Transactions on Power Electronics*, v. 12, n. 2, p. 243–252, 1997. 37

Chai, M.; Xiao, D.; Dutta, R.; Fletcher, J. E. Space vector pwm techniques for three-to-five-phase indirect matrix converter in the overmodulation region. *IEEE Transactions on Industrial Electronics*, v. 63, n. 1, p. 550–561, 2016. 35

Chen, Y.; Yu, X.; Li, Y. A failure mechanism cumulative model for reliability evaluation of a k-out-of-n system with load sharing effect. *IEEE Access*, v. 7, p. 2210–2222, 2019. ISSN 2169-3536. 60

Choi, J.; Han, B.; Kim, H. New scheme of phase-shifted carrier pwm for modular multilevel converter with redundancy submodules. *IEEE Transactions on Power Delivery*, v. 31, n. 1, p. 407–409, Feb 2016. ISSN 0885-8977. 57

Debnath, S.; Qin, J.; Bahrani, B.; Saeedifard, M.; Barbosa, P. Operation, control, and applications of the modular multilevel converter: A review. *IEEE Transactions on Power Electronics*, v. 30, n. 1, p. 37–53, 2015. 50

Dekka, A.; Wu, B.; Fuentes, R. L.; Perez, M.; Zargari, N. R. Evolution of topologies, modeling, control schemes, and applications of modular multilevel converters. *IEEE Journal of Emerging and Selected Topics in Power Electronics*, v. 5, n. 4, p. 1631–1656, Dec 2017. ISSN 2168-6777. 30, 43

Diab, M. S. I. M. *Modular multilevel converter designs for medium-voltage machine drives.* Thesis (PhD) — University Of Strathclyde, 3 2019. 39

Diaz, M.; Dobson, R. C.; Ibaceta, E.; Mora, A.; Urrutia, M.; Espinoza, M.; Rojas, F.; Wheeler, P. An overview of applications of the modular multilevel matrix converter. *Energies*, MDPI AG, v. 13, n. 21, p. 5546, Oct 2020. ISSN 1996-1073. 35, 36

Dickerson, J. A.; Ottaway, G. H. *Transformerless power supply with line to load isolation.* : U.S. Patent, 1971. 3 596 369. 40

Emery, R.; Eugene, J. Harmonic losses in lci-fed synchronous motors. *IEEE Transactions on Industry Applications*, v. 38, n. 4, p. 948–954, 2002. 36

Erickson, R. W.; Al-Naseem, O. A. A new family of matrix converters. In: *IECON'01. 27th Annual Conference of the IEEE Industrial Electronics Society*. 2001. v. 2, p. 1515–1520 vol.2. 35

Falck, J.; Felgemacher, C.; Rojko, A.; Liserre, M.; Zacharias, P. Reliability of power electronic systems: An industry perspective. *IEEE Industrial Electronics Magazine*, v. 12, n. 2, p. 24–35, June 2018. ISSN 1932-4529. 61

Fang Zheng Peng; Jih-Sheng Lai; McKeever, J.; VanCoevering, J. A multilevel voltage-source inverter with separate dc sources for static var generation. In: *IAS '95. Conference Record of the 1995 IEEE Industry Applications Conference Thirtieth IAS Annual Meeting*. 1995. v. 3, p. 2541–2548 vol.3. 41

Farias, J. V. M. *Reliability-Oriented Redundancy Design for Modular Multilevel Cascaded Converter-based STATCOMs*. Dissertation (Master) — CEFET-MG, Brasil, 2019. 66

Farias, J. V. M.; Cupertino, A. F.; Ferreira, V. N.; Pereira, H. A.; Seleme, S. I. Redundancy design for modular multilevel converter based statcoms. *Microelectronics Reliability*, v. 100-101, p. 113471, 2019. ISSN 0026-2714. 30th European Symp. on Rel. of Electron. Devices, Failure Physics and Analysis. 59, 61

Farias, J. V. M.; Cupertino, A. F.; Pereira, H. A.; Junior, S. I. S.; Teodorescu, R. On the redundancy strategies of modular multilevel converters. *IEEE Transactions on Power Delivery*, v. 33, n. 2, p. 851–860, April 2018. ISSN 0885-8977. 47, 49, 54, 57, 67

Fortes, G. O.; Mendes, M. A. S.; Cortizo, P. C. Integrated solution for driving series-connected igbts and its natural intrinsic balancing. *Energies*, MDPI AG, v. 12, n. 12, p. 2406, Jun 2019. ISSN 1996-1073. 38

Franquelo, L. G.; Rodriguez, J.; Leon, J. I.; Kouro, S.; Portillo, R.; Prats, M. A. M. The age of multilevel converters arrives. *IEEE Industrial Electronics Magazine*, v. 2, n. 2, p. 28–39, 2008. 39

Gemmell, B.; Dorn, J.; Retzmann, D.; Soerangr, D. Prospects of multilevel vsc technologies for power transmission. In: *IEEE/PES Transmission and Distribution Conference and Exposition*. 2008. p. 1–16. ISSN 2160-8555. 47

Guo, J.; Wang, X.; Liang, J.; Pang, H.; Gonçalves, J. Reliability modeling and evaluation of mmcs under different redundancy schemes. *IEEE Transactions on Power Delivery*, v. 33, n. 5, p. 2087–2096, 2018. 59, 64

Gyugyi, L.; Pelly, B. R. *Static Frequency Converter With Novel Voltage Control.* : U.S. Patent, 1969. 3 470 447). 34

Hagiwara, M.; Akagi, H. Control and experiment of pulsewidth-modulated modular multilevel converters. *IEEE Transactions on Power Electronics*, v. 24, n. 7, p. 1737–1746, 2009. 41, 50, 51

Hagiwara, M.; Hasegawa, I.; Akagi, H. Start-up and low-speed operation of an electric motor driven by a modular multilevel cascade inverter. *IEEE Transactions on Industry Applications*, v. 49, p. 1556–1565, July 2013. ISSN 0093-9994. 30, 42, 43, 48, 49, 50, 51, 56

Hagiwara, M.; Nishimura, K.; Akagi, H. A medium-voltage motor drive with a modular multilevel pwm inverter. *IEEE Transactions on Power Electronics*, v. 25, n. 7, p. 1786–1799, July 2010. ISSN 0885-8993. 43, 49, 51

Hammond, P. W. A new approach to enhance power quality for medium voltage ac drives. *IEEE Transactions on Industry Applications*, v. 33, n. 1, p. 202–208, 1997. 41

Harnefors, L.; Antonopoulos, A.; Norrga, S.; Angquist, L.; Nee, H. P. Dynamic analysis of modular multilevel converters. *IEEE Transactions on Industrial Electronics*, v. 60, n. 7, p. 2526–2537, July 2013. ISSN 0278-0046. 47, 54

Hiller, M.; Sommer, R.; Beuermann, M. Medium-voltage drives. *IEEE Industry Applications Magazine*, v. 16, n. 2, p. 22–30, 2010. 34

Hombu, M.; Ueda, S.; Ueda, A. A current source gto inverter with sinusoidal inputs and outputs. *IEEE Transactions on Industry Applications*, IA-23, n. 2, p. 247–255, 1987. 36

Huber, J. E.; Kolar, J. W. Optimum number of cascaded cells for high-power medium-voltage ac–dc converters. *IEEE Journal of Emerging and Selected Topics in Power Electronics*, v. 5, p. 213–232, March 2017. ISSN 2168-6777. 31, 54, 67

IEA. *World Energy Outlook 2019*. 2019. 27, 66

Ilves, K.; Harnefors, L.; Norrga, S.; Nee, H. Analysis and operation of modular multilevel converters with phase-shifted carrier pwm. In: *2013 IEEE Energy Conversion Congress and Exposition*. 2013. p. 396–403. 51

Ilves, K.; Norrga, S.; Harnefors, L.; Nee, H. On energy storage requirements in modular multilevel converters. *IEEE Transactions on Power Electronics*, v. 29, n. 1, p. 77–88, Jan 2014. ISSN 0885-8993. 53

Islam, M. R.; Guo, Y.; Zhu, J. A high-frequency link multilevel cascaded medium-voltage converter for direct grid integration of renewable energy systems. *IEEE Transactions on Power Electronics*, v. 29, n. 8, p. 4167–4182, Aug 2014. ISSN 0885-8993. 31, 52

Islam, M. R.; Guo, Y.; Zhu, J. A multilevel medium-voltage inverter for step-up-transformer-less grid connection of photovoltaic power plants. *IEEE Journal of Photovoltaics*, v. 4, May 2014. ISSN 2156-3381. 68

Islam Y. Guo, J. Z. M. R. *Power Converters for Medium Voltage Networks*. : Springer-Verlag Berlin Heidelberg, 2014. ISBN 9783662445297. 52, 53

Issouribehere, P. E.; Barbera, G. A.; Issouribehere, F.; Mayer, H. G. Power quality measurements and mitigation of disturbances due to pwm ac drives. In: *2008 IEEE Power and Energy Society General Meeting - Conversion and Delivery of Electrical Energy in the 21st Century*. 2008. p. 1–8. 27

Júnior, P. R. M.; Farias, J. V. M.; Cupertino, A. F.; Mendonça, G. A.; Stopa, M. M.; Pereira, H. A. Selection of the number of levels of a modular multilevel converter for an electric drive. In: *2019 COBEP/SPEC*. 2019. p. 1–6. 69

Kawamura, W.; Chen, K.; Hagiwara, M.; Akagi, H. A low-speed, high-torque motor drive using a modular multilevel cascade converter based on triple-star bridge cells (mmcc-tsbc). *IEEE Transactions on Industry Applications*, v. 51, n. 5, p. 3965–3974, 2015. 35

Kerkman, R.; Leggate, D.; Skibinski, G. Interaction of drive modulation and cable parameters on ac motor transients. In: *IAS '96. Conference Record of the 1996 IEEE Industry Applications Conference Thirty-First IAS Annual Meeting*. 1996. v. 1, p. 143–152 vol.1. 37

Klug, R. .; Klaassen, N. High power medium voltage drives - innovations, portfolio, trends. In: *2005 European Conference on Power Electronics and Applications*. 2005. p. 10 pp.–P.10. 13, 27, 30

Kolar, J. W.; Biela, J.; Waffler, S.; Friedli, T.; Badstuebner, U. Performance trends and limitations of power electronic systems. In: *2010 6th International Conference on Integrated Power Electronics Systems*. 2010. p. 1–20. 67

Konstantinou, G. S.; Ciobotaru, M.; Agelidis, V. G. Effect of redundant sub-module utilization on modular multilevel converters. In: *IEEE International Conference on Industrial Technology*. 2012. p. 815–820. 56, 57, 58

Korn, A. J.; Winkelnkemper, M.; Steimer, P. Low output frequency operation of the modular multi-level converter. In: *2010 IEEE Energy Conversion Congress and Exposition*. 2010. p. 3993–3997. 49

Kouro, S.; Malinowski, M.; Gopakumar, K.; Pou, J.; Franquelo, L. G.; Wu, B.; Rodriguez, J.; Pérez, M. A.; Leon, J. I. Recent advances and industrial applications of multilevel converters. *IEEE Transactions on Industrial Electronics*, v. 57, n. 8, p. 2553–2580, 2010. 30, 42

Kouro, S.; Rodriguez, J.; Wu, B.; Bernet, S.; Perez, M. Powering the future of industry: High-power adjustable speed drive topologies. *IEEE Industry Applications Magazine*, v. 18, n. 4, p. 26–39, July 2012. ISSN 1077-2618. 13, 27, 30, 34, 35, 36, 37, 39, 40, 41

Kumar, Y. S.; Poddar, G. Control of medium-voltage ac motor drive for wide speed range using modular multilevel converter. *IEEE Transactions on Industrial Electronics*, v. 64, n. 4, p. 2742–2749, April 2017. ISSN 0278-0046. 43

Kumar, Y. S.; Poddar, G. Medium-voltage vector control induction motor drive at zero frequency using modular multilevel converter. *IEEE Transactions on Industrial Electronics*, v. 65, n. 1, p. 125–132, Jan 2018. ISSN 0278-0046. 43

Lesnicar, A.; Marquardt, R. An innovative modular multilevel converter topology suitable for a wide power range. In: *2003 IEEE Bologna Power Tech Conference Proceedings,*. 2003. v. 3, p. 6 pp. Vol.3–. 42

Li, B.; Zhang, Y.; Yang, R.; Xu, R.; Xu, D.; Wang, W. Seamless transition control for modular multilevel converters when inserting a cold-reserve redundant submodule. *IEEE Transactions on Power Electronics*, v. 30, n. 8, p. 4052–4057, Aug 2015. ISSN 0885-8993. 57, 59

Li, B.; Zhou, S.; Xu, D.; Finney, S. J.; Williams, B. W. A hybrid modular multilevel converter for medium-voltage variable-speed motor drives. *IEEE Transactions on Power Electronics*, v. 32, n. 6, p. 4619–4630, June 2017. ISSN 0885-8993. 43

Li, Y.; Jones, E. A.; Wang, F. Circulating current suppressing control's impact on arm inductance selection for modular multilevel converter. *IEEE Journal of Emerging and Selected Topics in Power Electronics*, v. 5, n. 1, p. 182–188, 2017. 54

Liang, X.; Kar, N. C.; Liu, J. Load filter design method for medium-voltage drive applications in electrical submersible pump systems. *IEEE Transactions on Industry Applications*, v. 51, n. 3, p. 2017–2029, 2015. 27

Liu, G.; Xu, Z.; Xue, Y.; Tang, G. Optimized control strategy based on dynamic redundancy for the modular multilevel converter. *IEEE Transactions on Power Electronics*, v. 30, n. 1, p. 339–348, 2015. 59

Ma, K.; Blaabjerg, F. Modulation methods for three-level neutral-point-clamped inverter achieving stress redistribution under moderate modulation index. *IEEE Transactions on Power Electronics*, v. 31, n. 1, p. 5–10, 2016. 39

Malinowski, M.; Gopakumar, K.; Rodriguez, J.; Pérez, M. A. A survey on cascaded multilevel inverters. *IEEE Transactions on Industrial Electronics*, v. 57, n. 7, p. 2197–2206, 2010. 41

Marquadt, R. *Stromrichterschaltungen mit verteilten energiespeichern.* : German Patent, 2001. 20 011 030 31. 42

Marzoughi, A.; Burgos, R.; Boroyevich, D. Investigating impact of emerging medium-voltage sic mosfets on medium-voltage high-power industrial motor drives. *IEEE Journal of Emerging and Selected Topics in Power Electronics*, v. 7, n. 2, p. 1371–1387, June 2019. ISSN 2168-6777. 54, 67

Marzoughi, A.; Burgos, R.; Boroyevich, D.; Xue, Y. Design and comparison of cascaded h-bridge, modular multilevel converter, and 5-l active neutral point clamped topologies for motor drive applications. *IEEE Transactions on Industry Applications*, v. 54, n. 2, p. 1404–1413, Marchr 2018. ISSN 0093-9994. 31, 52

Mcmurray, W. *Inverter Circuits.* : U.S. Patent, 1965. 3 207 974. 37

Mcmurray, W. *Fast Response Stepped-Wave Switching Power Converter Circuit.* : U.S. Patent, 1971. 3 581 212. 39

Meynard, T. A.; Foch, H. Multi-level conversion: high voltage choppers and voltage-source inverters. In: *PESC '92 Record. 23rd Annual IEEE Power Electronics Specialists Conference*. 1992. p. 397–403 vol.1. 40

Munuswamy, I.; Wheeler, P. W. Matrix converter for more electric aircraft. In: DEKOULIS, G. (Ed.). *Aerospace Engineering*. Rijeka: IntechOpen, 2019. cap. 3. 35

Nabae, A.; Takahashi, I.; Akagi, H. A new neutral-point-clamped pwm inverter. *IEEE Transactions on Industry Applications*, IA-17, n. 5, p. 518–523, Sep. 1981. ISSN 1939-9367. 39

Nguyen, H.; Lee, H. A modulation scheme for matrix converters with perfect zero common-mode voltage. *IEEE Transactions on Power Electronics*, v. 31, n. 8, p. 5411–5422, 2016. 35

Novotny, W. D.; Lipo, T. A. *Vector Control and Dynamics of AC Drives*. : Clarendon Press, 1996. ISBN 9780198564393. 50

Okayama, H.; Uchida, R.; Koyama, M.; Mizoguchi, S.; Tamai, S.; Ogawa, H.; Fujii, T.; Shimomura, Y. Large capacity high performance 3-level gto inverter system for steel main rolling mill drives. In: *IAS '96. Conference Record of the 1996 IEEE Industry Applications Conference Thirty-First IAS Annual Meeting*. 1996. v. 1, p. 174–179 vol.1. 27

Okazaki, Y.; Kawamura, W.; Hagiwara, M.; Akagi, H.; Ishida, T.; Tsukakoshi, M.; Nakamura, R. Which is more suitable for mmcc-based medium-voltage motor drives, a dscc inverter or a tsbc converter? In: *2015 9th International Conference on Power Electronics and ECCE Asia (ICPE-ECCE Asia)*. 2015. p. 1053–1060. 35

Okazaki, Y.; Kawamura, W.; Hagiwara, M.; Akagi, H.; Ishida, T.; Tsukakoshi, M.; Nakamura, R. Experimental comparisons between modular multilevel dscc inverters and tsbc converters for medium-voltage motor drives. *IEEE Transactions on Power Electronics*, v. 32, n. 3, p. 1805–1817, 2017. 35

Pan, J.; Ke, Z.; Al Sabbagh, M.; Li, H.; Potty, K. A.; Perdikakis, W.; Na, R.; Zhang, J.; Wang, J.; Xu, L. 7-kv 1-mva sic-based modular multilevel converter prototype for medium-voltage electric machine drives. *IEEE Transactions on Power Electronics*, v. 35, n. 10, p. 10137–10149, 2020. 30, 42

Pedra, J.; Corcoles, F. Estimation of induction motor double-cage model parameters from manufacturer data. *IEEE Transactions on Energy Conversion*, v. 19, n. 2, p. 310–317, 2004. 63

Rissik, H. *Mercury-Arc Current Converters*. : Sir Isaac Pitman and Sons, 1935. 34

Rodriguez, J.; Bernet, S.; Wu, B.; Pontt, J. O.; Kouro, S. Multilevel voltage-source-converter topologies for industrial medium-voltage drives. *IEEE Transactions on Industrial Electronics*, v. 54, n. 6, p. 2930–2945, 2007. 41

Rodriguez, J.; Jih-Sheng Lai; Fang Zheng Peng. Multilevel inverters: a survey of topologies, controls, and applications. *IEEE Transactions on Industrial Electronics*, v. 49, n. 4, p. 724–738, 2002. 27, 30

Saad, H.; Guillaud, X.; Mahseredjian, J.; Dennetière, S.; Nguefeu, S. Mmc capacitor voltage decoupling and balancing controls. *IEEE Transactions on Power Delivery*, v. 30, n. 2, p. 704–712, April 2015. ISSN 0885-8977. 57, 59

Sahoo, S. K.; Bhattacharya, T. Phase-shifted carrier-based synchronized sinusoidal pwm techniques for a cascaded h-bridge multilevel inverter. *IEEE Transactions on Power Electronics*, v. 33, n. 1, p. 513–524, Jan 2018. ISSN 0885-8993. 51

Schmitt, B. P.; Sommer, R. Retrofit of fixed speed induction motors with medium voltage drive converters using npc three-level inverter high-voltage igbt based topology. In: *ISIE 2001. 2001 IEEE International Symposium on Industrial Electronics Proceedings*. 2001. v. 2, p. 746–751 vol.2. 27

Shammas, N. Y. A.; Withanage, R.; Chamund, D. Review of series and parallel connection of igbts. *IEE Proceedings - Circuits, Devices and Systems*, v. 153, n. 1, p. 34–39, 2006. 38

Sharifabadi, K.; Harnefors, L.; Nee, H. P.; Norrga, S.; Teodorescu, R. *Design, Control, and Application of Modular Multilevel Converters for HVDC Transmission Systems*. 2016. 60-132 p. 52, 54

Siddique, H. A. B.; Lakshminarasimhan, A. R.; Odeh, C. I.; De Doncker, R. W. Comparison of modular multilevel and neutral-point-clamped converters for medium-voltage grid-connected applications. In: *International Conference on Renewable Energy Research and Appl.* 2016. p. 297–304. 31, 68

Siemens. *Sinamics SM 120 CM*. 2018. Available in: <https://www.industry.siemens.com/drives/global/en/converter/mv-drives/Pages/sinamics-sm120-cm.aspx>. 43

Slabiak, W.; Lawson, L. J. Precise control of a three-phase squirrel-cage induction motor using a practical cycloconverter. *IEEE Transactions on Industry and General Applications*, IGA-2, n. 4, p. 274–280, 1966. 34

Son, G. T.; Lee, H. J.; Nam, T. S.; Chung, Y. H.; Lee, U. H.; Baek, S. T.; Hur, K.; Park, J. W. Design and control of a modular multilevel hvdc converter with redundant power modules for noninterruptible energy transfer. *IEEE Transactions on Power Delivery*, v. 27, n. 3, p. 1611–1619, July 2012. ISSN 0885-8977. 56, 57, 59

Steinke, J. K.; Steimer, P. K. Medium voltage drive converter for industrial applications in the power range from 0.5 mw to 5 mw based on a three-level converter equipped with igcts. In: *IEE Seminar PWM Medium Voltage Drives*. 2000. p. 6/1–6/4. 27

Stemmler, H. High-power industrial drives. *Proceedings of the IEEE*, v. 82, n. 8, p. 1266–1286, 1994. 34

Stemmler, H.; Guggenbach, P. Configurations of high-power voltage source inverter drives. In: *1993 Fifth European Conference on Power Electronics and Applications*. 1993. p. 7–14 vol.5. 29

Tai, B.; Gao, C.; Liu, X.; Chen, Z. A novel flexible capacitor voltage control strategy for variable-speed drives with modular multilevel converters. *IEEE Transactions on Power Electronics*, v. 32, n. 1, p. 128–141, 2017. 27, 30

Tolbert, L. M.; Fang Zheng Peng; Habetler, T. G. Multilevel converters for large electric drives. *IEEE Transactions on Industry Applications*, v. 35, n. 1, p. 36–44, 1999. 29

Tu, P.; Yang, S.; Wang, P. Reliability and cost based redundancy design for modular multilevel converter. *IEEE Transactions on Industrial Electronics*, p. 1–1, 2018. ISSN 0278-0046. 59, 60

Wang, H.; Liserre, M.; Blaabjerg, F.; Rimmen, P. P.; Jacobsen, J. B.; Kvisgaard, T.; Landkildehus, J. Transitioning to physics-of-failure as a reliability driver in power electronics. *IEEE Journal of Emerging and Selected Topics in Power Electronics*, v. 2, n. 1, p. 97–114, March 2014. ISSN 2168-6777. 61

Wang, H.; Ma, K.; Blaabjerg, F. Design for reliability of power electronic systems. In: *IECON 2012 - 38th Annual Conference on IEEE Industrial Electronics Society*. 2012. p. 33–44. 59

WEG. *Software de Dimensionamento WEG*. 2021. Available in: <https://sdw.weg.net/>. 72

Wheeler, J. C. G. Effects of converter pulses on the electrical insulation in low and medium voltage motors. *IEEE Electrical Insulation Magazine*, v. 21, n. 2, p. 22–29, 2005. 37

Wu, B.; Narimani, M. *High-Power Converters and AC Drives*. 2017. 1-16 p. 11, 28, 30, 43

Wu, B.; Pontt, J.; Rodriguez, J.; Bernet, S.; Kouro, S. Current-source converter and cycloconverter topologies for industrial medium-voltage drives. *IEEE Transactions on Industrial Electronics*, v. 55, n. 7, p. 2786–2797, 2008. 33, 34, 36, 37

Wu, B.; Rizzo, S.; Zargari, N.; Xiao, Y. An integrated dc link choke for elimination of motor common-mode voltage in medium voltage drives. In: *Conference Record of the 2001 IEEE Industry Applications Conference. 36th IAS Annual Meeting (Cat. No.01CH37248)*. 2001. v. 3, p. 2022–2027 vol.3. 37

Xiaoming Yuan; Barbi, I. Fundamentals of a new diode clamping multilevel inverter. *IEEE Transactions on Power Electronics*, v. 15, n. 4, p. 711–718, 2000. 40

Xu, C.; Dai, K.; Chen, X.; Kang, Y. Unbalanced pcc voltage regulation with positive- and negative-sequence compensation tactics for mmc-dstatcom. *IET Power Electronics*, v. 9, n. 15, p. 2846–2858, 2016. ISSN 1755-4535. 49

Zhu, N.; Xu, D.; Wu, B.; Zargari, N. R.; Kazerani, M.; Liu, F. Common-mode voltage reduction methods for current-source converters in medium-voltage drives. *IEEE Transactions on Power Electronics*, v. 28, n. 2, p. 995–1006, 2013. 29

Biography

Paulo Roberto Matias Júnior was born in Ubá-MG, Brazil in 1996. He received the B.S. degree in Electrical Engineering from the Universidade Federal de Viçosa, Viçosa-MG, Brazil in 2018. Currently, he is a collaborating researcher at Gerência de Especialistas em Eletrônica de Potência (GESEP), where he develops researches in the area of Electrical Drives and Power Electronics, with focus in Modular Multilevel Converters Based Electrical Drives.

E-mail: paulomatiaspq@gmail.com

Website: www.gesep.ufv.br

Research Gate: www.researchgate.net/profile/Paulo_Junior31

ORCID: 0000-0003-0023-2349